ARTICLE

KIF1Bβ mutations detected in hereditary neuropathy impair IGF1R transport and axon growth

Fang Xu[1], Hironori Takahashi[1], Yosuke Tanaka[1], Sotaro Ichinose[1], Shinsuke Niwa[1], Matthew P. Wicklund[2], and Nobutaka Hirokawa[1,3]

KIF1Bβ is a kinesin-3 family anterograde motor protein essential for neuronal development, viability, and function. KIF1Bβ mutations have previously been reported in a limited number of pedigrees of Charcot-Marie-Tooth disease type 2A (CMT2A) neuropathy. However, the gene responsible for CMT2A is still controversial, and the mechanism of pathogenesis remains elusive. In this study, we show that the receptor tyrosine kinase IGF1R is a new direct binding partner of KIF1Bβ, and its binding and transport is specifically impaired by the Y1087C mutation of KIF1Bβ, which we detected in hereditary neuropathic patients. The axonal outgrowth and IGF-I signaling of *Kif1b*−/− neurons were significantly impaired, consistent with decreased surface IGF1R expression. The complementary capacity of KIF1Bβ-Y1087C of these phenotypes was significantly impaired, but the binding capacity to synaptic vesicle precursors was not affected. These data have supported the relevance of KIF1Bβ in IGF1R transport, which may give new clue to the neuropathic pathogenesis.

Introduction

Kinesin superfamily proteins (KIFs) largely serve as microtubule molecular motors that transport essential cellular materials to specific destinations, while very little is known regarding how they regulate the cellular signal transduction cascades specifically involved in important cellular functions (Hirokawa et al., 2010; Hirokawa and Tanaka, 2015). KIF1Bβ is a kinesin-3 family member that plays an indispensable role in neuronal survival, morphogenesis, and function (Zhao et al., 2001). *Kif1b*−/− mice die soon after birth due to apnea. The brains of *Kif1b*−/− mice are reduced in volume by ∼10% compared with the brains of WT littermates. The cellularity, organization, and the development of the brain stem nuclei and commissural fibers are also significantly decreased. The dissociated hippocampal neuron culture shows severe neuronal death by day in vitro (DIV) 3, and KIF1Bβ expression restores neuron number. However, a distinct splicing isoform with a totally different cargo-binding domain, KIF1Bα, cannot restore the neuron number. In contrast, KIF1Bβ and its closely related motor protein KIF1A both transport synaptic vesicle precursors including synaptophysin, SV2, and synaptotagmin down the neuronal axons (Zhao et al., 2001) by binding to the dynamic adaptors Rab3A-GTP and differentially expressed in neoplastic versus normal cells protein (DENN)/MAPK-activating death domain (MADD; Niwa et al., 2008). In oligodendrocytes, KIF1Bβ is essential for *Mbp* and *36k* mRNA localization, and it has

a role in the development of myelinated axons in the central and peripheral nervous systems (Lyons et al., 2009).

Interestingly, the phenotypes of *Kif1b*−/− neurons are much more severe than those deficient of presynaptic proteins or adaptor proteins such as synaptophysin, synaptotagmin, SV2A or 2B, and Rab3A (Geppert et al., 1994a,b; McMahon et al., 1996; Crowder et al., 1999; Janz et al., 1999), suggesting that there may be a novel cargo of KIF1Bβ other than synaptic vesicle precursors that essentially regulates neuronal survival and axonal outgrowth.

Insulin-like growth factors (IGFs) control the growth and differentiation of neural cells, enhancing dendrite extension, axon elongation, synaptogenesis, spine formation, and myelination. IGF1R dominantly mediates the growth-promoting actions of IGF-I and IGF-II (O'Kusky and Ye, 2012). *Igf-I*–knockout (KO) mice and *Igf1r*-KO mice tend to die immediately after birth from respiratory failure, showing reduced brain sizes, muscle hypoplasia, reduced neuron numbers, and impaired commissural fiber formation (Liu et al., 1993; Beck et al., 1995). IGF1R is a heterotetrameric glycoprotein with paired disulfide-linked extracellular α- and transmembrane β-subunits (Baron-Van Evercooren et al., 1991). The binding of the α-subunit to IGF-I leads to the activation of the β-subunit kinase domain and subsequently transduces the signal to downstream MAPK and PI3K–Akt pathways (Kuemmerle and Murthy, 2001).

[1]Department of Cell Biology and Anatomy, Graduate School of Medicine, The University of Tokyo, Tokyo, Japan; [2]Department of Neurology, Penn State Hershey Medical Center, Hershey, PA; [3]Center of Excellence in Genome Medicine Research, King Abdulaziz University, Jeddah, Saudi Arabia.

Correspondence to Nobutaka Hirokawa: hirokawa@m.u-tokyo.ac.jp; M.P. Wicklund's present address is Department of Neurology, University of Colorado Denver, Aurora, CO.

IGF-I signaling was reported to play a role in neuronal survival in vivo and in vitro. Significant neuronal loss was reported in *Igf-I*–KO mice (Beck et al., 1995; Camarero et al., 2001) and *IGF1R*-deficient mice (Liu et al., 2009). In contrast, *IGF-I*–overexpressing transgenic mice showed a substantial increase in the number of brain neurons (Dentremont et al., 1999; O'Kusky et al., 2000; Hodge et al., 2005). IGF1R is required for the IGF-I–activated Akt survival cascade in neuronal cells (Dudek et al., 1997; Lu et al., 2008). Furthermore, IGF-I stimulates the axonal outgrowth of motor and sensory neurons (Özdinler and Macklis, 2006; Scolnick et al., 2008). Commissural fibers of *IGF-I*$^{-/-}$ mouse brains are greatly reduced in area and thickness compared with WT littermates (Beck et al., 1995). The IGF1R-mediated PI3K pathway is essential for the establishment of the polarity of hippocampal neurons (Sosa et al., 2006) and for regulating membrane expansion at the nerve growth cone, which is necessary for axonal outgrowth (Laurino et al., 2005). MAPK signaling has been also reported to promote axonal outgrowth (Forcet et al., 2002). Changes in serum IGF levels were found to be associated with neurodegeneration (Busiguina et al., 2000). Recent research also showed that treatment with recombinant human IGF-I ameliorates the symptoms of a mouse model of Rett Syndrome with IGF-I deficiency (Castro et al., 2014). Thus, the IGF-I signaling pathway is a potential therapeutic target for neurological disorders.

Charcot-Marie-Tooth (CMT) disease is one of the most common inherited peripheral neuropathies, with a prevalence of 1:2,500 (Skre, 1974) as the result of summing up the mutations in >30 genes (Saporta et al., 2011); this condition is also known as hereditary motor and sensory neuropathy. CMT disease is divided into two main types on the basis of electrophysiological properties and neuropathology: CMT1 and CMT2. Demyelinating CMT1 has a nerve conduction velocity <38 m/s, and axonal CMT2 has nerve conduction velocities >38 m/s. For CMT1, axonal loss occurs largely due to affected Schwann cells, whereas Mitofusin 2 (*MFN2*) mutations, which impair mitochondrial fusion and ER–mitochondria tethering, are responsible for the most common known axonal form of CMT2A2 (Züchner et al., 2004; Kijima et al., 2005; Lawson et al., 2005; Baloh et al., 2007). Although a *KIF1B* mutation in the same genomic interval was the first identified in a pedigree with CMT2A, only a few pedigrees with KIF1Bβ mutation for CMT2A1 have been reported until recently. We previously reported one CMT2A1 pedigree with the clinical mutation of KIF1Bβ-Q98L in the middle of the P loop, which is the conserved ATP binding site of the kinesin motor. This mutation significantly reduced ATPase activity, resulting in the perinuclear accumulation of the mutant protein (Zhao et al., 2001). In addition, compared with WT mice, 1-yr-old *Kif1b* heterozygous mice had significantly reduced retention times in the rotarod test (Zhao et al., 2001). The mutation E758D in KIF1Bβ was identified in a patient diagnosed with hereditary motor neuropathies with pyramidal signs, and the mutation V1358A was found for CMT2 with a limited penetrance (Drew et al., 2015).

In this study, we propose that the IGF1R-containing vesicle is a novel cargo of KIF1Bβ. We show that the IGF1Rβ subunit directly binds to the 885–1,410-aa domain located in the stalk domain of KIF1Bβ protein and is transported down the axon to augment ax-onal outgrowth. Furthermore, we detected the *a3260g* (Y1087C) mutation of human *Kif1bβ* gene in the patients from two independent pedigrees of hereditary neuropathy suffering from CMT2A symptoms including progressive muscle weakness and slight central nervous system defects. We show cell biological evidence that this Y1087C mutation significantly affects the IGF1R binding capacity of KIF1Bβ and that KIF1Bβ Y1087C is impaired in complementing the defects in IGF1R transport and axonal outgrowth of *Kif1b*$^{-/-}$ mouse primary hippocampal neurons. These data will newly propose that KIF1Bβ as a responsible gene preventing hereditary axonopathy through the association of its specific binding domain with IGF1R, which enhances the expression of IGF1R and the IGF-I–mediated signaling in the peripheral axon.

Results

KIF1B is essential for axonal outgrowth

We previously reported that the corpus callosum of *Kif1b*$^{-/-}$ mice was significantly malformed (Zhao et al., 2001), which was further confirmed by histological analyses (Fig. S1, A–D). We hypothesized that this is because of the impairment in axonal outgrowth. To evaluate it, we compared axonal outgrowth in vitro using dissociated hippocampal neurons from 17.5–d postcoitum (dpc) mouse brains. TagRFP was transiently transfected to show the morphology of single neurons at 1 d before the observation. The cells were then fixed and visualized by confocal microscopy using the 568-nm channel. We found that axonal outgrowth was significantly impaired in *Kif1b*$^{-/-}$ neurons at DIV2–3 (Fig. 1, A and B). In the knockdown experiments using the KIF1Bα- and -β–specific miRNA vectors, we found that the β-isoform of KIF1B was specifically responsible for this impairment in axonal outgrowth, which could be rescued by expression of RNAi-resistant KIF1Bβ (Fig. 1, C–E; and Fig. S1, E and F). Using terminal deoxynucleotidyl transferase dUTP nick-end labeling (TUNEL) staining of dissociated hippocampal neuron culture at DIV3, we found that neurite-bearing *Kif1b*$^{-/-}$ neurons were not largely apoptotic, excluding the nonspecific effect of apoptosis as the cause of the axonal elongation phenotype (Fig. 1 F). However, the ratio of apoptotic cells in *Kif1b*$^{-/-}$ neurons was significantly higher than that in *Kif1b*$^{+/+}$ neurons (Fig. 1 G), consistent with our previous data (Zhao et al., 2001).

IGF1R is specifically associated with KIF1Bβ

Considering that these phenotypes were most similar to those of *IGF1R*-KO mice (Liu et al., 1993, 2009), we sought to investigate whether IGF1R is a novel cargo of KIF1Bβ. Because the nascent IGF1R protein undergoes proteolysis to generate an N-terminal extracellular α-subunit (IGF1Rα) that has a ligand-binding domain and a C-terminal transmembrane β-subunit (IGF1Rβ) that is extracellularly linked to the α-domain by disulfide bonds and possesses an intracellular catalytic domain (Massagué and Czech, 1982), the intracellular domain (ICD) of IGF1Rβ is considered the only portion exposed to the cytoplasm.

First, we conducted yeast two-hybrid analysis to explore the direct binding capacity between KIF1Bβ and IGF1R. Using the ICD of IGF1Rβ as the prey, blue colonies indicating a positive signal were successfully formed with the indicated bait fragments of
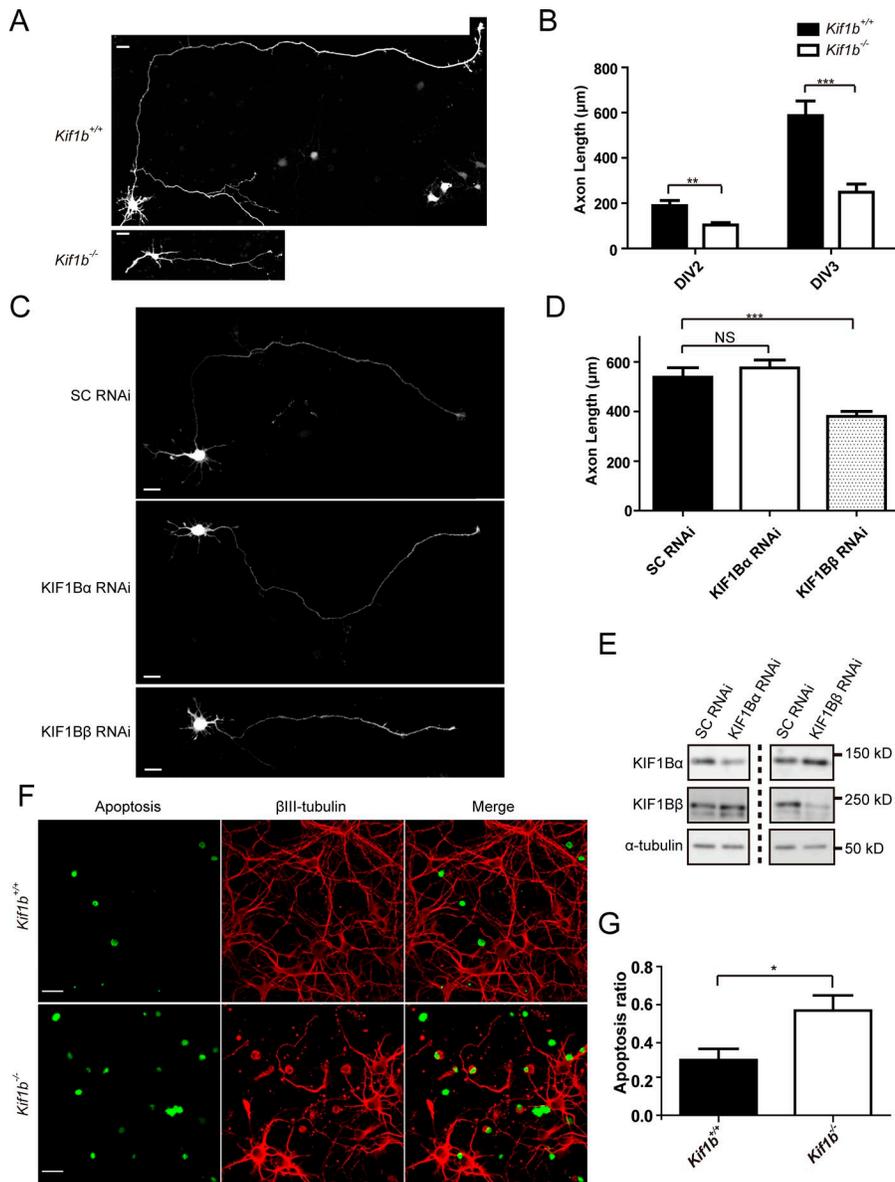
Xu et al.
The KIF1Bβ kinesin transports IGF1R down the axon

Journal of Cell Biology 3481
https://doi.org/10.1083/jcb.201801085

Figure 1. **KIF1Bβ is responsible for axonal elongation. (A and B)** Fluorescent micrographs of the hippocampal neurons of *Kif1b*^{+/+} and *Kif1b*^{−/−} mice at DIV3 (A). The neurons were plated at 8.6×10^4 cells/cm^2 and transfected with TagRFP accompanied by the quantification of axon lengths at DIV2 and 3 (B). The fluorescence microscopy data were collected using LSM710 or 780 confocal microscopes using Plan Apochromat 40×/1.4 or 40×/1.3 objectives, and the data are represented as the mean ± SEM. Bars, 25 μm. n = 21–25. **, $P < 0.01$; ***, $P < 0.001$, one-sided unpaired Welch's t test. **(C and D)** Fluorescent micrographs of DIV4 hippocampal neurons electroporated with the indicated miRNA vectors fused with TurboRFP at DIV0 using a Plan Apochromat 20×/0.8 objective (C) accompanied with the statistics of the longest neurite lengths (D). Note that KIF1Bβ knockdown significantly reduced neurite elongation. Bars, 20 μm. n = 55–90. ***, $P < 0.001$; ns, $P > 0.05$; one-sided Dunnett's method. **(E)** IB verifying the effects of KIF1Bα and KIF1Bβ knockdown vectors. N1E-115 cells were transfected with the respective miRNA vectors, lysed 2 d after transfection, and subjected to IB. Scrambled (SC) miRNA was used as a negative control. **(F and G)** TUNEL staining of the dissociated hippocampal neurons of *Kif1b*^{+/+} and *Kif1b*^{−/−} mice at DIV3 counterstained with an anti–β3-tubulin antibody (F) and quantified (G). Despite the significantly higher apoptosis rate in *Kif1b*^{−/−} neurons (G), note that the cells with long neurites are not largely apoptotic (F). Bar, 25 μm. n = 5–6 fields of vision. *, $P < 0.05$, one-sided unpaired Welch's t test.

the mouse KIF1Bβ stalk domain (Fig. 2 A). The binding domain of KIF1Bβ was thus minimized to 885–1,410 aa. However, mouse KIF1A 836–1,346 aa, which was homologous to mouse KIF1Bβ 885–1,410 aa, did not result in blue colony formation (Fig. S2, A and B), suggesting that IGF1Rβ specifically binds to KIF1Bβ instead of KIF1A. The stalk domain of KIF1Bβ shares a high homology with the corresponding domain of KIF1A, with a sequence identity of 65%. Because we found a nonconserved 20-aa stretch just before the core-binding residue Tyr1087 (Fig. S2 A), it is reasonable to hypothesize that these two motors have different binding specificities.

Second, this binding was confirmed by vesicle immunoprecipitation (IP) using newly established *Kif1bβ-EGFP*–knock-in mice, of which hippocampal neurons represented axonal transport of fluorescent organelles at ~1 μm/s (Fig. S2, C–F; Video 1). We immunoprecipitated the whole-brain lysates of adult *Kif-1bβ*^{GFP/GFP} and *Kif1bβ*^{+/+} mice using an anti-GFP antibody. The immunoprecipitates were labeled against GFP, KIF1Bβ, and IGF1Rα,

and this labeling specifically showed the association between KIF1Bβ-EGFP and IGF1R-associated vesicles (Fig. 2 B).

Third, we conducted a vesicle coflotation assay. Adult WT mouse brains were homogenized in Hepes-sucrose buffer, and the S1 fraction was subjected to Nycodenz density-gradient differential centrifugation (Fig. 2 C). The results showed that IGF1R and synaptophysin cofloted with KIF1Bβ.

To evaluate whether the interaction is direct or not, we next performed a pulldown assay using purified recombinant proteins. FLAG-tagged ICD of IGF1Rβ purified from the HEK293 cell could significantly bind to purified GST-tagged KIF1Bβ 885–1,410 aa compared with the purified GST-only as a negative control (Fig. 2 D).

Finally, we conducted live imaging. KIF1Bβ-EGFP and signal peptide (SP)-IGF1Rβ-RFP expression vectors were cotransfected into dissociated hippocampal neurons at DIV5, and the neurons were observed 2 d later using a spinning-disk confocal microscope to assess the comigration of these two proteins (Fig. 2 E and
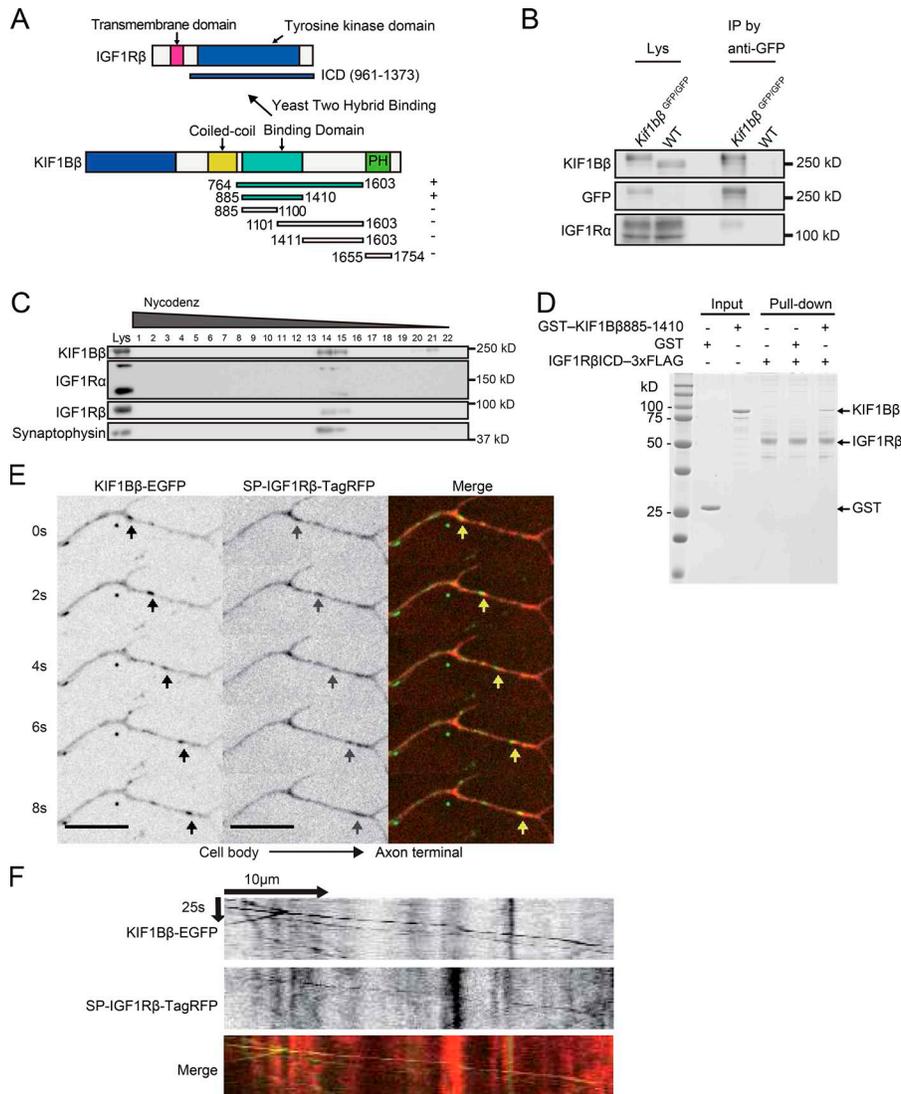
Figure 2. **IGF1R is a novel cargo of KIF1Bβ.** **(A)** Yeast two-hybrid assays assessing the direct binding between the ICD (961–1,373 aa) of mouse IGF1Rβ and various deletion mutants of mouse KIF1Bβ. Note that the 885–1,410-aa region within the KIF1Bβ stalk domain is the minimal essential region for its binding. PH, Pleckstrin homology. **(B)** Endogenous vesicle IP. IB of the brain lysates (Lys) of *Kif1bβ*^{GFP/GFP} and *Kif1bβ*^{+/+} (WT) mice and their immunoprecipitates using an anti-GFP antibody (IP by anti-GFP) labeled with the indicated antibodies. **(C)** Nycodenz gradient vesicle flotation assay of adult mouse brain lysates labeled with the indicated antibodies. Note that KIF1Bβ, IGF1Rα, IGF1Rβ, and synaptophysin are detected in the same fractions 14–15. **(D)** A Coomassie Brilliant Blue–stained gel for a pulldown assay between purified GST–KIF1Bβ885–1,410 and IGF1RβICD–3×FLAG showing their direct interaction. **(E and F)** Double-color time-lapse fluorescence images of a dissociated hippocampal neuron at DIV7 transfected with KIF1Bβ-EGFP and SP-IGF1Rβ-TagRFP using spinning-disk confocal microscopy equipped with 100×/1.46 Plan Apochromat oil-immersion objective lens (E) and its kymograph (F). The cell body is on the left side. Bars, 10 μm. Note that the speed of the comigrating vesicle (arrows in E) is ∼1 μm/s. See Video 2.

Video 2). Kymograph analyses suggested that the comigration speeds of these vesicles were ∼1 μm/s (Fig. 2 F), comparable with the previously measured velocity of KIF1Bβ (Zhao et al., 2001). To confirm that IGF1R is transported by KIF1Bβ, we transfected *Kif1b*^{+/+}, *Kif1b*^{+/−}, and *Kif1b*^{−/−} hippocampal neurons with SP-IGF1Rβ-RFP and compared the number of anterograde transport of IGF1R. *Kif1b*^{+/−} neurons showed less transport than *Kif1b*^{+/+} neurons (Fig. S2, G–J). Furthermore, little transport was observed in *Kif1b*^{−/−} neurons. These data indicate that IGF1R requires KIF1Bβ to be transported down the axon. Altogether, these data suggest that the stalk domain of KIF1Bβ is associated with membrane vesicles containing IGF1R through the ICD of IGF1Rβ.

Decreased surface expression of IGF1R in *Kif1b*^{−/−} neurons

To explore the physiological relevance of KIF1B to the IGF1R distribution, we dissected hippocampal neurons from *Kif1b*^{+/+} and *Kif1b*^{−/−} mouse embryos at 17.5 dpc, cultured them for 2 d upon dissociation, and then fixed and stained them with an anti-IGF1Rα antibody with permeabilization. We found that the axonal but not the total amount of the IGF1R was significantly decreased in the *Kif1b*^{−/−} neurons at DIV2 (Fig. S3, A–C). To evaluate the sur-face expression of IGF1R, we next performed immunostaining without permeabilization. As a result, the surface IGF1R levels both in the cell body and in the brightest neurite of *Kif1b*^{−/−} hippocampal neurons were also significantly lower than those of *Kif1b*^{+/+} neurons at an early developmental stage (Fig. 3, A and B).

Because the precise quantification of the transport was difficult in the dissociated culture due to the crossing and overlapping of the neurites, we next quantified the amount of IGF1R using microfluidic chambers with 450-μm-long microgrooves to specifically examine the distal axons. The neurons were plated in the left main channel of the device, and their axons were allowed to extend into the microgrooves for ∼1 wk until both *Kif1b*^{+/+} and *Kif1b*^{−/−} axons reached the right ends. The chamber was then carefully detached from the coverslip, and the cells attached to the cover glasses were fixed, permeabilized with saponin, and stained with the anti-IGF1Rα and βIII-tubulin antibodies (Fig. 3 C). The results of the statistical analysis revealed that axonal IGF1Rα staining in *Kif1b*^{−/−} neurons was significantly lower than that in *Kif1b*^{+/+} neurons (Fig. 3 D).

To confirm the reduction of surface expression of IGF1R in *Kif1b*^{−/−} neurons, we next conducted a surface biotinylation assay
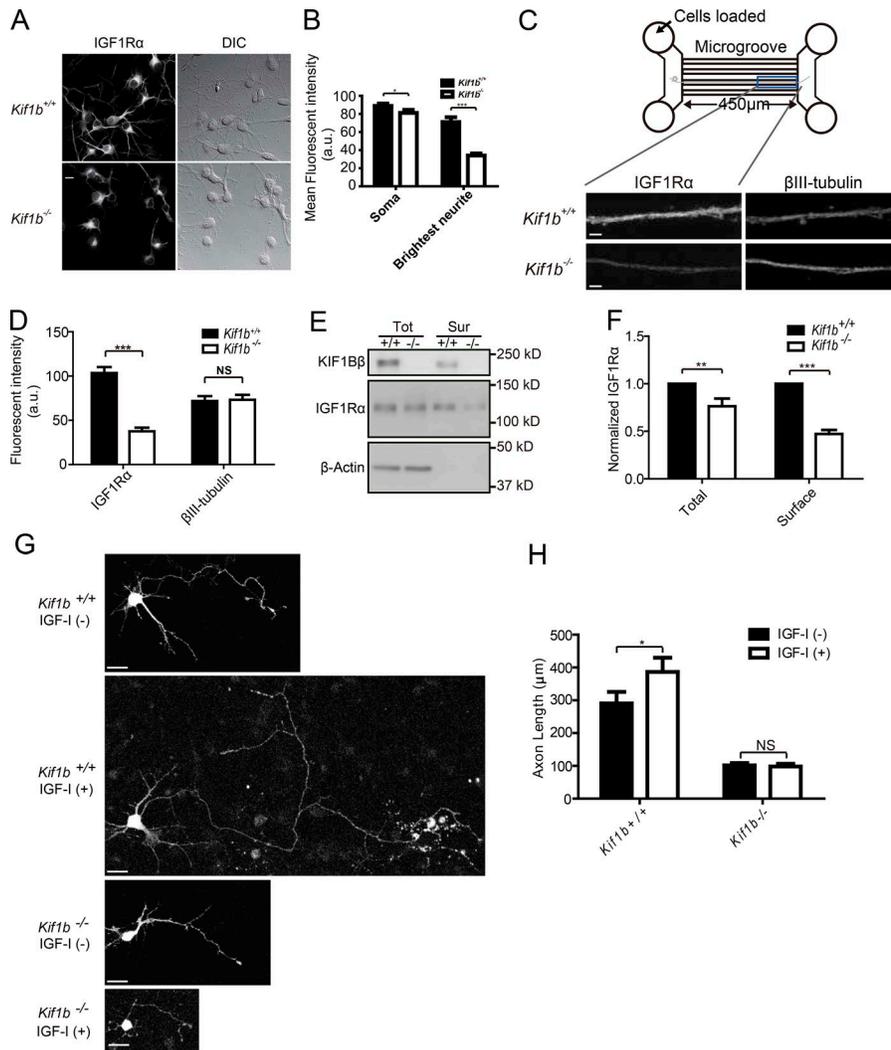
Figure 3. **Decreased surface expression of IGF1R in *Kif1b*⁻/⁻ mouse neuronal axons. (A and B)** Surface immunocytochemistry of *Kif1b*⁺/⁺ and *Kif1b*⁻/⁻ mouse hippocampal neurons at DIV2 against IGF1Rα accompanied by the respective differential interference contrast (DIC) images taken using a Plan Apochromat 20×/0.8 objective (A) and quantification (B). Cells were plated at 8.6 × 10⁴ cells/cm². Note the significant decrease in the surface IGF1Rα staining both in the cell body and neurites. Bar, 10 µm. *n* = 31–42. *, P < 0.05; ***, P < 0.001, one-sided unpaired Welch's *t* test. **(C and D)** Axonal immunocytochemistry against IGF1Rα and βIII-tubulin of *Kif1b*⁺/⁺ and *Kif1b*⁻/⁻ mouse hippocampal neurons at DIV7 using microfluidic chamber culture (C) and the quantification (D). **(C)** Top: Schematic view of the device. Bottom: Immunofluorescent images with the cell body on the left. Note that axonal IGF1Rα but not βIII-tubulin of *Kif1b*⁻/⁻ neurons was significantly decreased compared with that of *Kif1b*⁺/⁺ neurons. Bar, 5 µm. *n* = 17–26. ***, P < 0.001, one-sided unpaired Welch's *t* test. **(E and F)** The surface biotinylation assay of primary cultured mouse cortical neurons of the indicated genotypes (E) and its quantification (F). Note a significant decrease in the surface IGF1Rα level by the KIF1B deficiency. Tot, total lysate; Sur, surface fraction. *n* = 8. **, P < 0.01, ***, P < 0.001, one-sided paired Welch's *t* test. **(G and H)** Fluorescent micrographs of DIV3 hippocampal neurons of the indicated genotypes transfected with EGFP and cultured with or without 10 nM IGF-I in the medium (G) accompanied with the statistical analysis (H). The axons of *Kif1b*⁺/⁺ neurons with 10 nM IGF-I in the culture were significantly longer than the ones without IGF-I. However, the IGF-I stimulation was less effective in *Kif1b*⁻/⁻ neurons. Bars, 25 µm. *n* = 29–40. *, P < 0.05; ns, P > 0.05, one-sided unpaired Welch's *t* test.

using cortical neurons of *Kif1b*⁺/⁺ and *Kif1b*⁻/⁻ mouse embryos at 17.5 dpc. The neurons were cultured in 10-cm dishes for ~7 d. The membrane proteins were biotinylated, prepared for immunoblotting (IB), and normalized with the β-actin levels of the input. The IGF1R level in the cell surface fraction of *Kif1b*⁻/⁻ neurons was significantly lower than that of *Kif1b*⁺/⁺ neurons (Fig. 3 E). The statistical analysis was obtained from eight repetitions of the IB results of three independent experiments (Fig. 3 F). Interestingly, KIF1Bβ was detected in the surface fractions. Considering that another molecular motor cytoplasmic dynein has been reported to be associated with the plasma membrane and tethers microtubules, KIF1Bβ might be recruited by these cortically-tethered microtubules (Hendricks et al., 2012). We also noted that the total amount of IGF1R of *Kif1b*⁻/⁻ neurons tended to slightly decrease at DIV7, but its amplitude was substantially less than that in the cell surface fractions. This finding suggests the existence of a self-activation loop for *IGF1R* expression, possibly through the PKC signaling pathway (Ververis et al., 1993), which may secondarily down-regulate *IGF1R* transcription because of impaired downstream signaling during middle developmental stage.

To investigate whether the impairment in axonal outgrowth in the *Kif1b*⁻/⁻ neuron is correlated with the reduction of surface expression of IGF1R, we treated *Kif1b*⁺/⁺ and *Kif1b*⁻/⁻ neurons with a moderate level of IGF-I. As expected, *Kif1b*⁻/⁻ neurons were insensitive to IGF-I, and no significant axonal elongation was observed, whereas *Kif1b*⁺/⁺ neurons treated with IGF-I successfully developed the axons (Fig. 3, G and H). These data suggest that KIF1Bβ is essential for the surface expression of IGF1R in the axon and plays an essential role in the axon development.

Impaired IGF-I signaling in KIF1Bβ-deficient neurons
To examine the possible changes in IGF1R signal transduction caused by KIF1B deficiency, dissociated hippocampal neurons were cultured for 3 d, starved for 2 h without serum or B27 supplement, and stimulated for 5 min with 5 nM IGF-I. The cells were then fixed and subjected to immunostaining using an anti-pAkt antibody. Upon IGF-I stimulation, the pAkt level in the *Kif1b*⁺/⁺ cell body was substantially enhanced, while this enhancement was significantly impaired in the *Kif1b*⁻/⁻ neuron (Fig. 4, A and B). We next investigated the change in pERK levels as an indicator of MAPK signaling downstream to the IGF1R signaling. IGF-I stimulation significantly increased the pERK levels in the *Kif1b*⁺/⁺ neurons in 5 min compared with those in *Kif1b*⁻/⁻ neurons (Fig. S4, A and B).
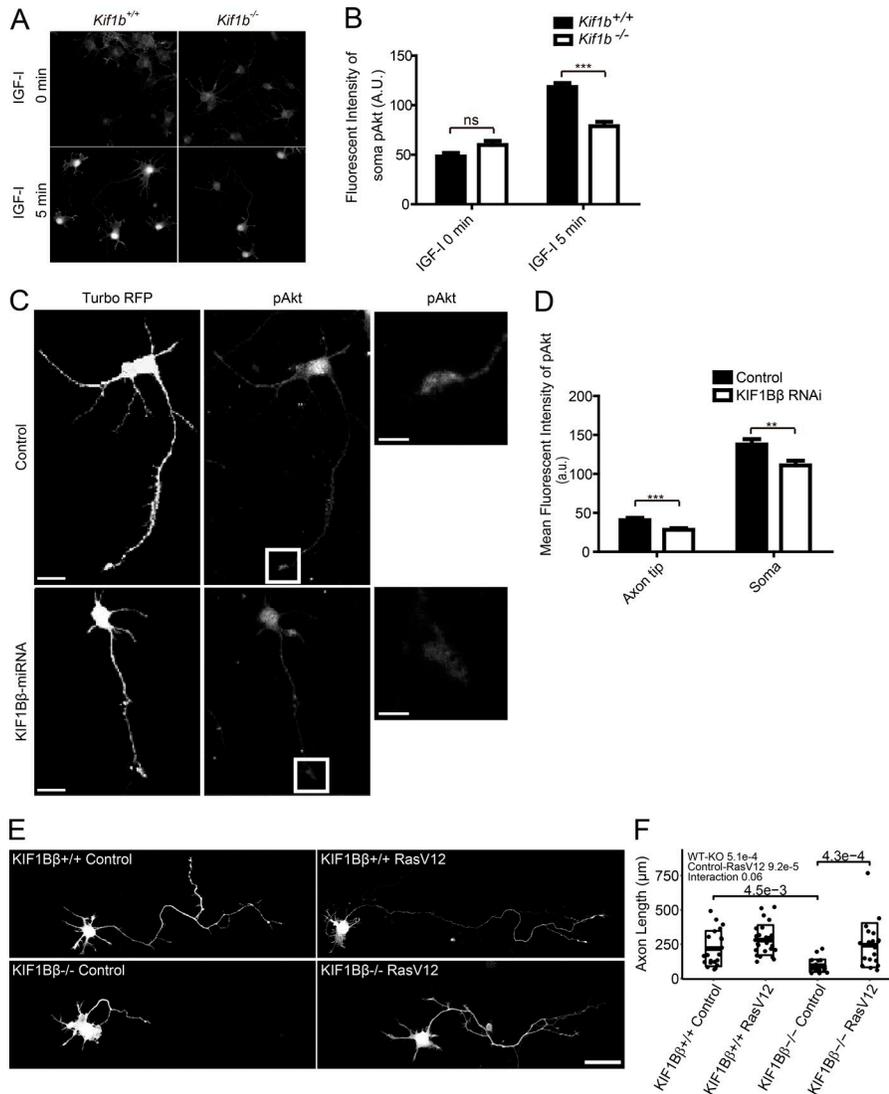
Figure 4. **Decreased IGF1R/PI3K signaling by KIF1Bβ deficiency. (A and B)** Immunocytochemistry against pAkt (Thr308) of primary mouse hippocampal neurons of the indicated genotypes at DIV3 with IGF-I stimulation for 0 and 5 min (A) and its quantification at the cell body (B). Bar, 25 μm. n = 8–50. ***, $P < 0.001$; ns, $P > 0.05$, one-sided unpaired Welch's t test. **(C and D)** Immunocytochemistry against pAkt of IGF-I–stimulated DIV4 mouse hippocampal neurons electroporated with the indicated TurboRFP-conjugated miRNA vectors (C) and its quantification (D). Open boxes in the middle panels in C indicate the axon tips magnified in the rightmost panels. Bars: 20 μm (low-magnification images); 5 μm (high-magnification images). n = 24–56. **, $P < 0.01$, ***, $P < 0.001$, one-sided unpaired Welch's t test. **(E)** Fluorescent micrographs of DIV3 $Kif1b^{+/+}$ and $Kif1b^{-/-}$ hippocampal neurons transfected with EGFP as a control or Ras V12 IRES EGFP taken using a Plan Apochromat 20×/0.8 objective. Bars, 20 μm. **(F)** Quantification of axon lengths of $Kif1b^{+/+}$ + control (n = 25), $Kif1b^{+/+}$ + Ras V12 (n = 22), $Kif1b^{-/-}$ + control (n = 22), and $Kif1b^{-/-}$ + Ras V12 (n = 21). Plots and mean ± SD. Two-way ANOVA post hoc Tukey's test was used. Before ANOVA tests, the normal distribution was tested using Kolmogorov–Smirnov test throughout the figures. Note that Ras V12 IRES EGFP significantly rescued neurite elongation deficits in $Kif1b^{-/-}$ hippocampal neurons.

The responsible isoform of KIF1B was further specified into KIF1Bβ using RNA interference. WT dissociated hippocampal neurons were electroporated with the TurboRFP-conjugated miRNA vector for the control or KIF1Bβ, plated, cultured for 4 d, and then starved for 2 h. The cells were treated with or without 10 nM IGF-I stimulation for 5 min and then fixed and immunostained using the anti-pAkt and anti-pERK antibodies. KIF1Bβ knockdown led to significant reduction in pAkt and pERK levels both in the axon tips and in the cell bodies (Fig. 4, C and D; and Fig. S4, C and D).

We further evaluated whether the impairment in IGF1R/PI3K signal transduction affected the axon outgrowth in $Kif1b^{-/-}$ neurons. $Kif1b^{-/-}$ neurons transfected with constitutively active Ras V12, which is upstream to the PI3K–Akt and ERK signaling (Castellano and Downward, 2011; Tanaka et al., 2016), showed a significant increase of the axon length compared with the $Kif1b^{-/-}$ neurons at DIV3 (Fig. 4, E and F). Interestingly, the effect of Ras V12 was more evident in the $Kif1b^{-/-}$ neurons than $Kif1b^{+/+}$ neurons. These data indicate that KIF1Bβ is essential for IGF1R-mediated PI3K and ERK signaling and axonal outgrowth.

KIF1Bβ-Y1087C mutation detected in patients affects IGF1R binding capacity

Coincidentally, we identified two hereditary neuropathy pedigrees carrying the same KIF1Bβ mutation Y1087C (Fig. 5, A and B; Table 1) by exome sequencing of 33 CMT2/neuropathy-related genes (Table 2). According to the in silico pathogenicity evaluation programs *PP2* and *SIFT*, this KIF1Bβ mutation was the only one with disease-causing capacity in the single-nucleotide polymorphisms (SNPs) within these 33 genes including MFN2.

Because Tyr1087 is located in the middle of the IGF1R minimal binding sequence (885–1,410 aa) as above, we conducted GST-pulldown assays to investigate whether this Y1087C mutation affected the binding capacity of KIF1Bβ to IGF1R and synaptic vesicle precursors. WT adult mouse brain lysates were pulled down against GST-fused mouse KIF1Bβ 885–1,410 aa with or without the Y1087C mutation. The mutated KIF1Bβ 885–1,410 aa (Y1087C) fragment tended to exhibit a lower binding capacity to both of the IGF1R subunits than WT KIF1Bβ 885–1,410 aa. However, the binding capacities to the synaptic vesicle precursor pro-

Xu et al.
The KIF1Bβ kinesin transports IGF1R down the axon

Journal of Cell Biology
https://doi.org/10.1083/jcb.201801085

3485

Table 1. Summary of the clinical manifestations

| Patient 1	Basic information	Left-handed Caucasion male, 55 yr old (on diagnosis)
	Major problems	Progressive, symmetric, length dependent, sensory motor, predominantly axonal polyneuropathy with intermittent cranial nerve involvement, Bell's palsy, etc.
	Laboratory tests and diagnosis	Hearing loss; normal MRI of the brain; severe symmetric sensorimotor length-dependent, axonal polyneuropathy with acute and chronic features; mixed axonal and demyelinating neuropathy of the right radial nerve; median nerve conduction velocity 38.9m/s; diagnosed with CMT2 disease
	Family history	No symptom of three brothers, three sisters and mother; however, father died from an accident at a young age
Patient 2	Basic information	Left-handed Caucasian male, 40 yr old (on diagnosis)
	Major problems	Mental retardation, bipolar disorder, hypertension, cystic kidney disease, and right basal ganglia lacune
	Laboratory tests and diagnosis	An MRI of the brain showing thinned corpus callosum in the posterior half; electromyography and nerve conduction velocity measurements implying predominantly length-dependent, axonal, sensorimotor polyneuropathy; diagnosed with autosomal-dominant CMT2 disease
	Family history	Brother having the constellation of mental retardation, psychiatric disease, kidney disease, and axonal CMT disease; mother having a history of CMT disease and mild cognitive dysfunction
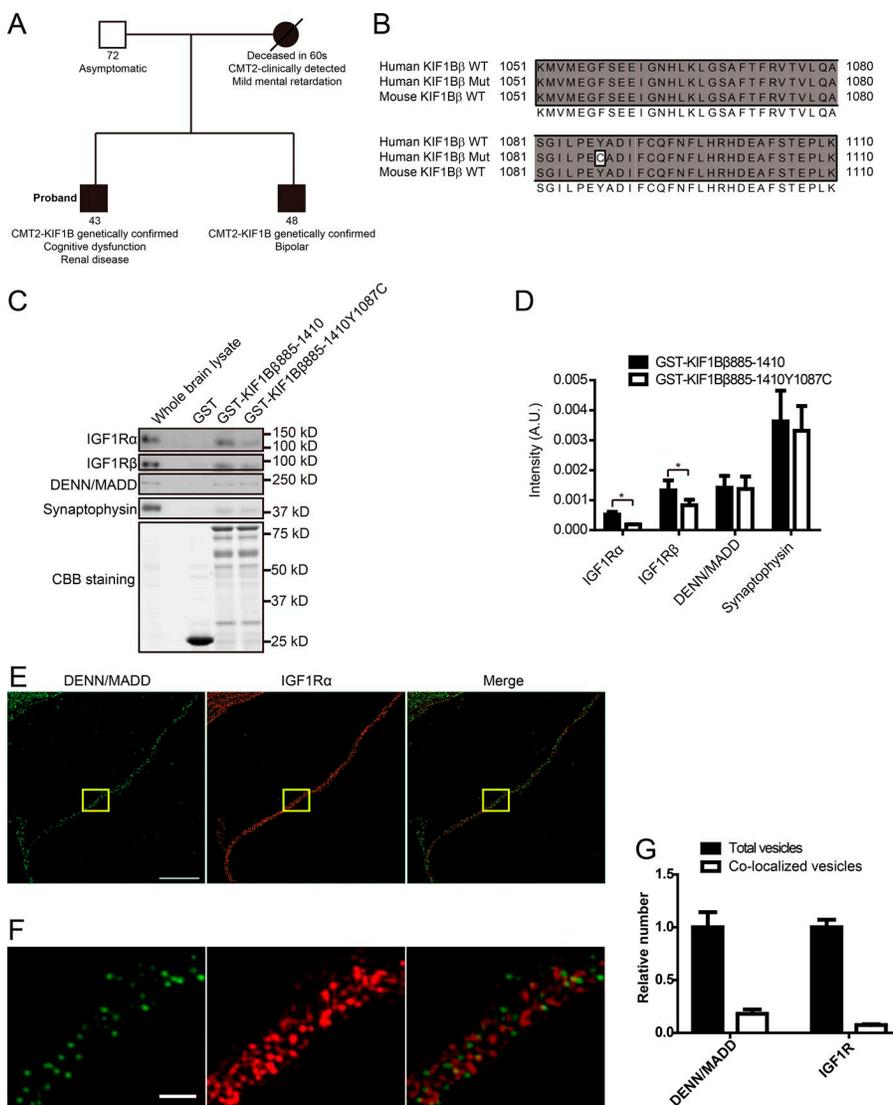
Figure 5. **KIF1Bβ-Y1087C protein reduced the affinity to IGF1R. (A)** An American pedigree of CMT2A1 patients. The proband (Patient 2 in Table 1) was a 43-yr-old male with KIF1Bβ Y1087C mutation genetically confirmed, and so was his 48-yr-old brother. Their mother was also clinically diagnosed as CMT2 and deceased in her 60s, while their father was asymptomatic and healthy at the age of 72 yr. **(B)** Amino acid sequence alignment of the human KIF1Bβ stalk region spanning the Y1087C mutation between WT and the new CMT2A pedigree (Mut) together with WT mouse KIF1Bβ. **(C and D)** The GST-pull-down assay of mouse brain lysates using GST-mouse KIF1Bβ 885–1,410 aa with or without the Y1087C mutation immunoblotted with the indicated antibodies (C) and its quantification (D). The signal intensities were normalized by the respective GST-tagged protein expression levels. Note that the binding capacity to IGF1R but not that to DENN/MADD or synaptophysin was significantly decreased by the mutation. CBB, Coomassie Brilliant Blue. $n = 3$. *, $P < 0.05$, one-sided paired Welch's t test. **(E–G)** Superresolution immunocytochemistry of hippocampal neurons at DIV7 against DENN/MADD (green) and IGF1Rα (red) at low (E) and high (F) magnifications, respectively, followed by the quantification (G). Bars: 10 µm (E); 1 µm (F). Note that there are few colocalizing vesicles with ~17% for DENN/MADD ($n = 142$) and 8% for IGF1R ($n = 299$) of the total vesicles, respectively.

Table 2. **The characterization of the CMT2A mutation**

	Mutated gene	Position	Amino acid change	Zygosity	Inheritance	1000 Genomes Minor Allele Frequency
Confirmed mutation	*KIF1B*	CHR1: 10387567	Y1087C	Heterozygote	Autosomal dominant	0.0395
Analyzed genes	*AARS* (601065), *ATL1* (606439), *DNM2* (602378), *DNMT1* (126375), *DYNC1H1* (600112), *EGR2* (129010), *FGD4* (611104), *GARS* (600287), *GDAP1* (606598), *GJB1* (304040), *GLA* (300644), *HSPB1* (602195), *HSPB8* (608014), *KIF1B* (605995), *LITAF* (603795), *LMNA* (150330), *LRSAM1* (610933), *MED25* (610197), *MFN2* (608507), *MPZ* (159440), *MTMR2* (603557), *NDRG1* (605262), *NEFL* (162280), *PMP22* (601097), *PRX* (605725), *RAB7A* (602298), *SBF2* (607697), *SCN9A* (603415), *SH3TC2* (608206), *SPTLC2* (605713), *TRPV4* (605427), *TTR* (176300), and *YARS* (603623)					

tein synaptophysin and the adaptor protein DENN/MADD were likely unaltered by the Y1087C mutation (Fig. 5, C and D).

To determine whether IGF1R and synaptic vesicle precursors are transported on the same vesicles, we then conducted fluorescence immunocytochemistry of WT dissociated hippocampal neurons against DENN/MADD and IGF1R and observed them using superresolution structured illumination microscopy (SR-SIM). DENN/MADD and IGF1R scarcely colocalized with each other (Fig. 5, E–G). These data collectively suggest that IGF1R directly binds to a specific domain in KIF1Bβ stalk domain including Tyr1087 and is transported independently from synaptic vesicle precursors. The mutation Y1087C in KIF1Bβ critically and specifically affected the IGF1R transport and, accordingly, may affect downstream IGF-I signaling to enhance the neuropathic symptoms.

KIF1Bβ-Y1087C is impaired in complementing KO neuron phenotypes

To further investigate the functional deficits of the KIF-1Bβ-Y1087C mutation, we conducted rescue experiments using *Kif1b⁻/⁻* hippocampal neurons. First, to assess axon length, dissociated neurons were transfected using the respective EG-FP-tagged expression vectors together with a TagRFP expression vector at DIV1, fixed at DIV3, and analyzed for axon lengths using confocal microscopy observations with the 568-nm excitation. Transfection of mouse WT KIF1Bβ restored axonal outgrowth. However, transfection of KIF1Bβ-Y1087C and KIF1Bβ-Q98L mutants, KIF1Bα, and KIF1A significantly failed in this complementation capacity compared with the WT KIF1Bβ, while KIF-1Bβ-Y1087C could partially rescue it (Fig. 6 A). The expression of recombinant proteins of the predicted lengths was confirmed by IB (Fig. 6 B), and the statistical analyses of the axon lengths are shown in Fig. 6 C. Knockdown rescue experiments also confirmed the dysfunction of KIF1Bβ-Y1087C (Fig. S1, E and F). Knockdown-resistant KIF1Bβ WT successfully rescued the impairment in axon outgrowth, while the neurons transfected with KIF1Bβ-Y1087C showed shorter axon lengths than those with WT.

To evaluate whether the impairment of axon outgrowth in the neurons expressing KIF1Bβ-Y1087C was caused by the impaired IGF1R/PI3K signal transduction, we next quantified the pAkt signals in the neurons transfected with miRNA and knockdown-resistant KIF1Bβ. Knockdown of KIF1Bβ caused a reduction in the pAkt levels in the axon shaft when stimulated with IGF-I, while KIF1A knockdown as a control showed no significant

changes, which was consistent with the results mentioned above (Fig. 6, D and E). Besides, the neurons expressing KIF1Bβ-Y1087C also showed a significant reduction in pAkt levels, whereas KIF-1Bβ-WT successfully rescued this reduction. Considering that the total Akt level was not changed in any condition (Fig. S5, A and B), these data suggest that IGF1R-mediated PI3K signal transduction was incomplete in the *Kif1b⁻/⁻* neurons expressing KIF1Bβ-Y1087C and thus, the incomplete signaling cascade might impair the axon outgrowth.

Y1087C mutation impaired the IGF1R transport

As we mentioned, the impairment in axon outgrowth and the reduction of pAkt levels in *Kif1b⁻/⁻* neurons may be induced by the decreased transport of IGF1R. Likewise, we hypothesized that KIF1Bβ-Y1087C could not transport IGF1R sufficiently. To compare the activity of KIF1Bβ mutants for the surface presentation of IGF1R, *Kif1b⁻/⁻* hippocampal neurons were cultured at a moderate density, transfected with 3× FLAG-tagged expression vectors together with a TagRFP expression vector at DIV1, fixed at DIV4, and immunostained using an anti-IGF1Rα antibody without permeabilization. *Kif1b⁺/⁺* neurons were also stained as a positive control. The axonal surface IGF1R expression levels at ~100 µm distal from the cell body were analyzed. The overexpression of mouse KIF1Bβ significantly rescued the axonal IGF1R expression level compared with control, while other constructs had lesser capacity for this complementation, similar with the case of axonal outgrowth above (Fig. 7, A and B). The expression of recombinant proteins of the predicted lengths was confirmed by IB (Fig. 7 C), and the statistical analysis of the axonal surface IGF1R levels at 100 µm distal from the cell body is shown in Fig. 7 D. These data indicate that the *Kif1b⁻/⁻* neurons expressing KIF1Bβ-Y1087C could not still sufficiently transport IGF1R.

To obtain further confirmation, we next observed the IGF1R transport in the *Kif1b⁻/⁻* hippocampal neurons expressing KIF1Bβ WT or Y1087C with live imaging. Because of the reduction in endogenous KIF1Bβ and IGF1R levels, the *Kif1b⁻/⁻* neurons provided a very suitable system for live imaging of transfected proteins (Fig. 8, A–C). As a result, the number of transported IGF1R-containing vesicles was not rescued in the neurons expressing KIF1Bβ-Y1087C, whereas it was rescued in the neurons expressing WT (Fig. 8 D). To obtain further insight of the mutant, we analyzed the transport quantitatively. The ratio of anterograde over retrograde transports of IGF1R was not significantly altered, suggesting that the retrograde
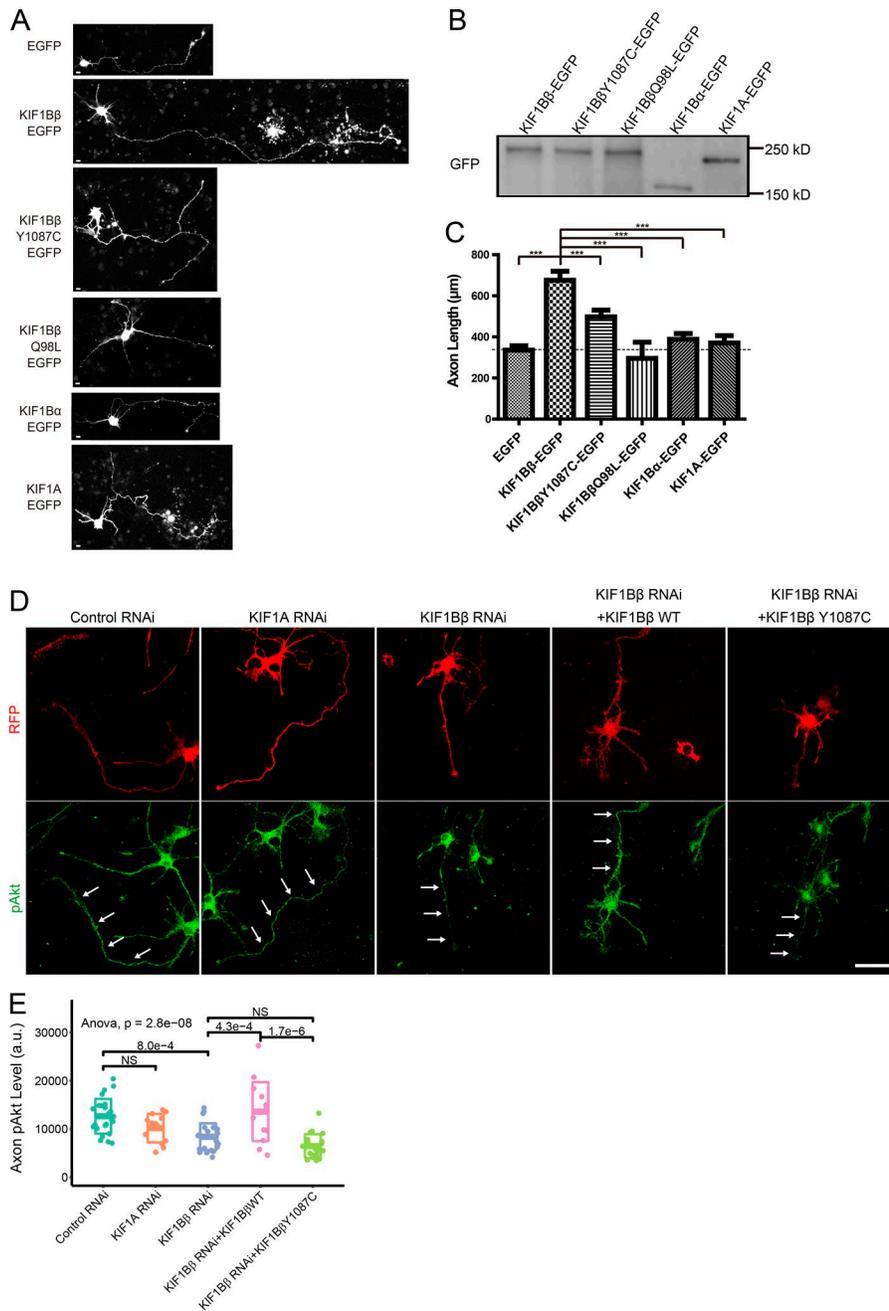
Figure 6. **KIF1Bβ-Y1087C reduced the capacity to complement axonal outgrowth. (A)** Fluorescent images of TagRFP-labeled *Kif1b*$^{-/-}$ mouse–dissociated hippocampal neurons at DIV3 expressing the indicated constructs for 48 h. Neurons were plated at a cell density of 8.6×10^4 cells/cm^2 for this assay. Bars, 10 μm. **(B)** Anti-GFP IB of the lysates of Neuro2A cells expressing the indicated constructs. **(C)** Quantification of the axon lengths. Mean ± SEM. *n* = 23–132. ***, P < 0.001, one-way ANOVA with post Dunnett's multiple comparisons. **(D and E)** Immunocytochemistry against pAkt (Thr308) of DIV3 hippocampal neurons electroporated with the control miRNA, KIF1A miRNA, and KIF1Bβ miRNA vectors together with or without miR-NA-resistant KIF1Bβ WT and Y1087C mutation at DIV0 (D) accompanied with the statistics of the mean pAkt level along the axon per unit length (E). Note that miRNA-immune KIF1Bβ significantly rescued neurite elongation deficits in *Kif1b*$^{-/-}$ hippocampal neurons. Arrows indicate axons. Bars, 50 μm. Plots and mean ± SD. Two-sided one-way ANOVA post hoc Tukey's test was used. Control RNAi, *n* = 25; KIF1A RNAi, *n* = 13; KIF1Bβ RNAi, *n* = 24; KIF1Bβ RNAi + KIF1Bβ WT, *n* = 14; KIF1Bβ RNAi + KIF1Bβ Y1087C, *n* = 20. The P values are indicated in the graph.

transport was proportionally impaired because of the reduction of IGF1R levels in the distal part of the axon in the neurons expressing the Y1087C mutant (Fig. 8 E). The velocity of KIF1Bβ was not significantly different either between WT and Y1087C or between the KIF1Bβ vesicles with and without IGF1R (Fig. 8 F). These data indicate that neither Y1087C mutation or the IGF1R interaction affected the motor activity. However, the ratio of comigrating over total KIF1Bβ-containing vesicles was significantly reduced in the neurons expressing Y1087C (Fig. 8 G). These results suggested that Y1087C could not gain the sufficient affinity to IGF1R. Thus, KIF1Bβ-Y1087C failed in transporting IGF1R to the axon. These mutation analyses in vivo confirmed that the IGF1R is a novel cargo of KIF1Bβ, and a disorder of this transport inhibited the IGF-I signaling and

proper axon outgrowth. Because KIF1Bβ-Y1087C mutation in the hereditary neuropathy patients partially but significantly affected these capacities, it probably enhances the pathogenesis of neuropathic symptoms in those patients.

Discussion

KIF1Bβ has been reported to transport synaptic vesicle precursors including synaptophysin, SV2, and synaptotagmin through the regulatory adaptors Rab3-GTP and DENN/MADD (Niwa et al., 2008). KIF1Bβ also transports dendritically localized mRNPs and is recruited to synapses in an activity-dependent manner (Charalambous et al., 2013). In oligodendrocytes, KIF1Bβ is involved in the localization of *Mbp* and *36k* mRNA and is essential
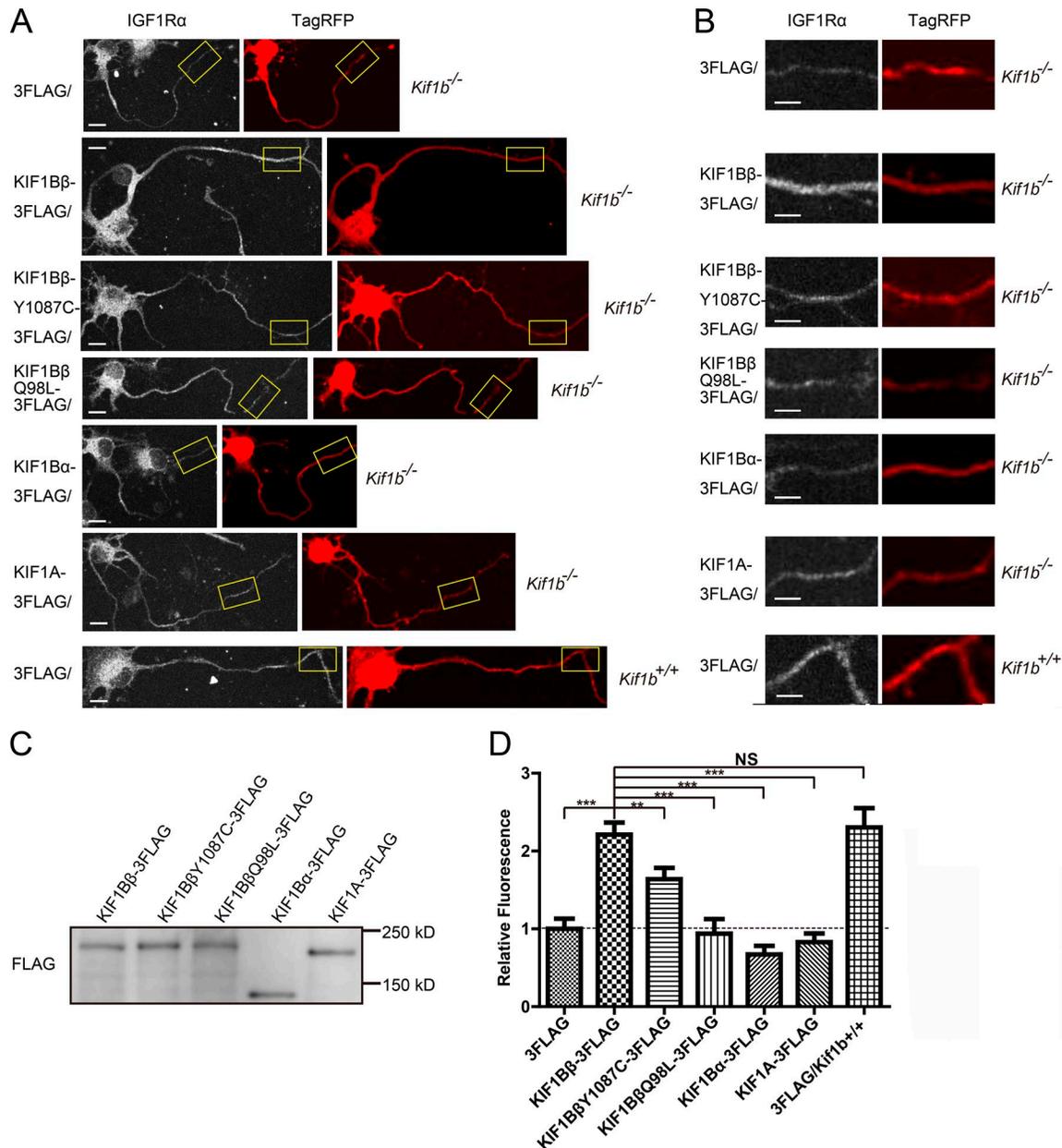
Figure 7. **KIF1Bβ-Y1087C reduced the capacity to complement surface IGF1Rα expression. (A and B)** Fluorescent images of the surface immunocytochemistry against IGF1Rα of *Kif1b*⁻/⁻ and *Kif1b*⁺/⁺ mouse–dissociated hippocampal neurons at DIV4 (left) together with the images of the transfection marker TagRFP (right) expressing the indicated constructs for 3 d. The neurons were plated at a cell density of 2.6 × 10⁴ cells/cm². Axonal regions at ∼100 µm apart from the somata (A, boxes) are enlarged in B. Bars: 10 µm (A); 5 µm (B). **(C)** Anti-DDDDK (FLAG) IB of the lysates of Neuro2A cells expressing the indicated constructs. **(D)** Quantification of the axonal surface IGF1Rα fluorescence intensities in B. n = 30–122. **, $P < 0.01$; ***, $P < 0.001$; ns, $P > 0.05$. Mean ± SEM. Two-sided one-way ANOVA with post Dunnett's multiple comparisons was adopted.

for the development of myelinated axons (Lyons et al., 2009). However, transport defects in these cargos cannot explain the phenotypes of *Kif1b*⁻/⁻ neurons, i.e., severe apoptosis and impaired axonal outgrowth; therefore, the existence of an unknown cargo promoting cell viability and axonal outgrowth has long been expected.

In this study, we first identified the association of IGF1R with KIF1Bβ using yeast two-hybrid, vesicle IP, coflotation, pulldown assay, and comigration experiments, and we also detected impairments in the surface presentation of IGF1R in *Kif1b*⁻/⁻ neuronal axons, suggesting that IGF1R is a novel cargo of KIF1Bβ. These

data clarify some of the missing information. IGF1R specifically bound to KIF1Bβ 885–1,410 aa, and coincidentally, we identified human pedigrees of CMT2A carrying the Y1087C mutation of KIF1Bβ, which turned out to specifically impair its binding capacity to IGF1R.

We have established a mechanistic link between KIF1Bβ-mediated axonal outgrowth and the IGF-I signaling pathway and propose the hypothesis that KIF1Bβ transports IGF1R in axons to stimulate axonal outgrowth. Because cell density can also affect cell outgrowth, in our research, a higher cell density was applied to compensate for apoptosis and its effect on axonal outgrowth
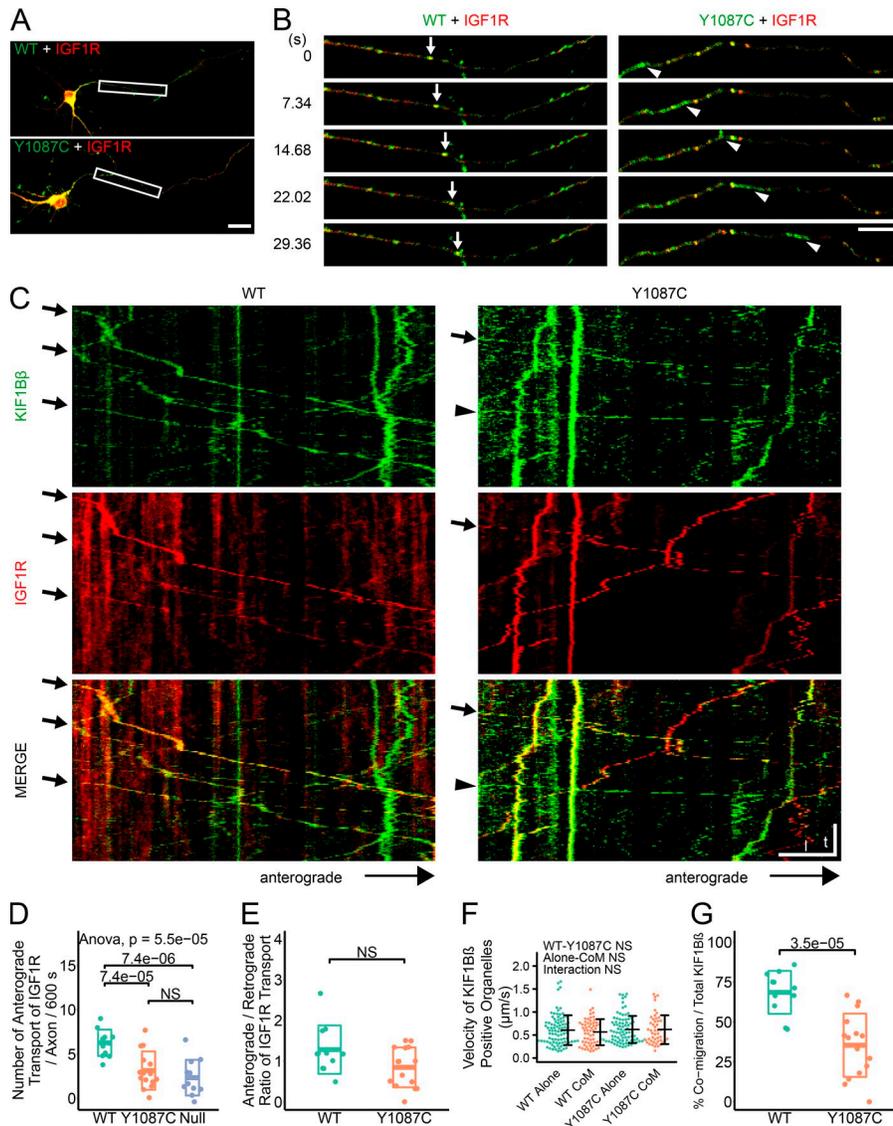
Figure 8. **Y1087C mutant affects comigration between KIF1Bβ and IGF1R. (A)** *Kif1b*^{-/-} hippocampal neurons (DIV8) coexpressing KIF-1Bβ-EGFP (WT or Y1087C) and SP-IGF1Rβ-RFP. The boxed regions were analyzed. **(B)** Sequential records of representative IGF1Rβ comigration with KIF1Bβ (arrows) and representative movement of KIF1Bβ-1087C alone (arrowheads). **(C)** The individual kymograph patterns of KIF1Bβ (WT or Y1087C), SP-IGF1Rβ, and their merged image. Arrows indicate representative comigration. Arrowheads indicate the movement of KIF1Bβ-Y1087C alone. **(D)** Quantification of anterograde transport of IGF1R in *Kif1b*^{-/-} neurons transfected with KIF1Bβ WT (*n* = 10), KIF1Bβ Y1087C (*n* = 15), and null (*n* = 12). Plots and mean ± SD. Two-sided one-way ANOVA post hoc Tukey's test was used. The P values are indicated in the graph. **(E)** Ratio of anterograde/retrograde transport of SP-IGF1Rβ-RFP. Plots and mean ± SD. *n* = 11–15. *, P > 0.05; ns, P > 0.05, one-sided Welch's *t* test. **(F)** Velocity of four types of KIF1Bβ movements in anterograde, KIF1Bβ WT, or Y1087C with or without IGF1R. CoM, comigration. Plots and mean ± SD. Two-way ANOVA post hoc Tukey's test was used. **(G)** Ratio of comigration to total KIF1Bβ moving in anterograde. Plots and mean ± SD. One-sided Welch's *t* test was used. *n* = 11–15. The P values are indicated in the graph. Bars: 20 µm (A); 10 µm (B and *l* in C); 100 s (*t* in C).

due to the lowered cell density (Fig. 1 F). Because dissociated hippocampal culture contains growth factor–secreting cells such as astrocytes, a higher density might provide a sufficient concentration of growth factors for the survival of *Kif1b*^{-/-} neurons. Furthermore, a low transfection efficiency of hippocampal neurons and evidence for impaired responsiveness to exogenous IGF-I (Fig. 4) suggested that the rescue of axonal outgrowth was primarily caused in a cell-autonomous way to increase the responsiveness to IGF-I.

CMT2 is defined as axonal hereditary neuropathy with a normal range of axon conduction speeds but exhibits severe axonal degeneration (Bucci et al., 2012). There are several pedigrees of CMT2A with *MFN2* point mutations (Züchner et al., 2004; Kijima et al., 2005; Lawson et al., 2005; Baloh et al., 2007); however, *MFN2* as well as >30 related genes were intact in our newly identified CMT2A pedigrees. Both of these pedigrees coincidentally carried the KIF1Bβ mutation of Y1087C, which strengthens the previously known mechanistic link between CMT2A and KIF1Bβ (Zhao et al., 2001; Drew et al., 2015). We present in vitro evidence that this mutation functionally impairs the capacity of KIF1Bβ

for specific binding and transport of IGF1R down the axons to affect IGF-I/IGF1R signaling, in contrast with previous negative predictions (Ho et al., 2017). Our in vitro evidence suggested that this mutation is at least responsible for increasing susceptibility to neuropathies by reducing the IGF-I signal transduction.

IGF-mediated MAPK and PI3K–Akt signal transduction has long been known to be essential for neuronal survival and axonal development (Beck et al., 1995; Dudek et al., 1997; Camarero et al., 2001; Özdinler and Macklis, 2006; Scolnick et al., 2008; Liu et al., 2009). Besides, changes in serum IGF levels were found to be associated with neurodegeneration (Busiguina et al., 2000). We have shown in this study that the IGF-mediated signaling is significantly affected by KIF1B deficiency (Figs. 4 and S4), and overexpression of Ras V12 that directly stimulates MAPK and PI3K signaling pathways (Kuemmerle and Murthy, 2001; Castellano and Downward, 2011) could rescue the axonal outgrowth phenotype (Fig. 3). Thus, deficiency in IGF1R signaling could provide a better explanation of the cause of neurodegeneration and impaired axonal elongation in *Kif1b*^{-/-} mice. These data will also stimulate future translational research into the activation

of the KIF1Bβ/IGF1R cascade to protect neurons against hereditary neuropathies.

Interestingly, IGF1R did not bind to the corresponding region of KIF1A (Fig. S2). This finding was consistent with the fact that KIF1A expression did not restore either axonal outgrowth or axonal surface IGF1R expression in *Kif1b*^{−/−} neurons (Figs. 6 and 7). Although KIF1A is very similar to KIF1Bβ and synergistically transports synaptic vesicle precursors (Niwa et al., 2008), we recently proposed that instead of KIF1Bβ, only KIF1A transports the nerve growth factor (NGF) receptor TrkA through the Rab3-GTP adaptor (Tanaka et al., 2016). As we have identified in this study that only KIF1Bβ transports the IGF-I receptor IGF1R by the direct binding of the stalk domain, KIF1A and KIF1Bβ may complementarily transport different receptor tyrosine kinases down the axons to respectively augment the NGF and IGF signaling pathways. Although both kinesin-3 motors are highly expressed in adult brains, dorsal root ganglion neurons express KIF1Bβ only in the juvenile or regenerating stages and solely express KIF1A in the mature stage (Takemura et al., 1996; Gumy et al., 2011; Tanaka et al., 2016). Furthermore, we previously identified that another kinesin-3 motor, KIF16B, transports fibroblast growth factor receptor for stem cell differentiation and proliferation (Ueno et al., 2011). Because FGF-, IGF-, and NGF-mediated transmembrane receptor tyrosine kinase pathways have been reported to sequentially and cooperatively enhance neuronal differentiation and survival through modality-specific adaptor proteins (Recio-Pinto et al., 1986; Nakafuku et al., 1992; Jones et al., 2003), the down-regulation of KIF1Bβ in adult peripheral nervous system may provide a hint to the answers of long-standing questions such as why the symptoms of CMT disease are peripheral dominant even though the responsible genes are ubiquitously expressed (Sullivan et al., 2008; Bucci et al., 2012) and why axonal regeneration and axonal outgrowth are generally suppressed in the adult central nervous system (Raivich and Makwana, 2007; Wu et al., 2007; Huebner and Strittmatter, 2009; Luigetti et al., 2016). Among these three kinesin-3 motors, the direct interaction of KIF1Bβ with the cargo was first identified in this study, and it is unique compared with the other two kinesin-3 motors, suggesting divergence in the transport regulation mechanism.

Materials and methods

Mice
Kif1b-KO mice have been previously described (Zhao et al., 2001). Mouse brain histology was performed using paraffin sections as previously described (Zhao et al., 2001). *Kif1bβ-EGFP*–knock-in mice were generated by using the gene-targeting vector (Fig. S2), which was electroporated in C57BL/6N strain mouse–derived RENKA embryonic stem cells (kindly provided by K. Sakimura, Niigata University, Niigata, Japan) selected for *neo*[R] homologous recombinant clones by Southern blotting using a DNA radioprobe (a *Kif1b* genomic fragment 130,394–131,090 nt; RefSeq expression no. NC_000070.6) according to methods previously described (Mishina and Sakimura, 2007). C57BL/6J, C57BL/6N, and ICR mice were purchased from CLEA Japan. The KO and knock-in mice were maintained in a C57BL/6J or C57BL/6N background in a specific pathogen-free environment under a 14/10-h light/

dark cycle. All animal experiments were conducted under The University of Tokyo's restrictions and permissions regarding animal experimentation (notification numbers 1722T124, 1722T126, M-P15-118, and M-P15-119).

Genotyping PCR
For genotyping PCR of *Kif1b*-KO mice, tail biopsy lysates were subjected to PCR as previously described (Zhao et al., 2001). For that of *Kif1bβ-EGFP* knock-in mice, the lysates were subjected to PCR using AmpliTaq DNA polymerase (PerkinElmer) on a thermal cycler (GeneAmp PCR system 9700; PerkinElmer). For amplifying the knock-in allele, the samples were cycled at 94°C for 30 s, 62°C for 30 s, and 72°C for 30 s for 30 cycles using the following primer sets: *EGFP-F*, 5′-CCATGGTGAGCAAGGGCGAGG AGCTGTTCA-3′, and *EGFP-R*, 5′-TCATGTGGTCGGGGTAGCGGC TGAAGCACT-3′, to reveal a 240-bp product. For the WT allele, they were cycled at 94°C for 30 s, 56.4°C for 30 s, and 72°C for 30 s for 30 cycles using the following primer sets: *KIF1Bβ-F*, 5′-TGT TTAGGAGCGTAGAAGCCTGG-3′, and *KIF1Bβ-R*, 5′-GTGTGAGTG TGAGTGTGTATGGACG-3′, to reveal a 386-bp product.

Expression and knockdown vectors
To construct mouse IGF1R deletion expression vectors, mouse *Igf1r* cDNA (IMAGE: 8861891; Open Biosystems) was amplified by PCRs using KOD polymerase (Toyobo) and KAPA HiFi DNA polymerase (KAPA Biosystems). For comigration experiments, *SP* (the first 30 residues of IGF1R) and *Igf1rβ* were amplified with PCR and ligated into the *pTagRFP-N* (Evrogen) vector using the *Bgl*II and *Hin*dIII sites or *Hin*dIII and *Eco*RI sites, respectively. Mouse *Kif1bβ* cDNA (Zhao et al., 2001), mouse *Kif1a* cDNA (Niwa et al., 2008), and human *KIF1Bα* cDNA (Niwa et al., 2008) were subcloned into the *pEGFP-N1* vector (Takara Bio Inc.) and a *3× FLAG (DYKDDDDK)-N1* vector (modified from *pEGFP-N1* vector) using the *Nhe*I and *Sma*I sites or *Nhe*I and *Hin*dIII sites, respectively. Mouse *Kif1b* cDNA was mutated using the QuikChange II XL kit (200522; Agilent Technologies) respectively with the following primer sets: 5′-CCAGCGGGATCCTTCCAGAGTGTGCAG ACATCT-3′ (sense) and 5′-AGATGTCTGCACACTCTGGAAGGA TCCCGCTGG-3′ (antisense) for introducing a Y1087C mutation, and 5′-CTTTGCCTATGGGCTGACTGGTGCTGGGA-3′ (sense) and 5′-TCCCAGCACCAGTCAGCCCATAGGCAAAG-3′ (antisense) for a Q98L mutation. For the GST-pulldown assay, mouse *Kif1bβ* 885–1,410 aa cDNA with or without the Y1087C mutation was subcloned into the *pGEX-6P-3* vector (GE Healthcare) using the *Eco*RI and *Not*I sites. The expression of these vectors was verified by IB using 293A cell lysates that were transfected with a Lipofectamine LTX reagent (Thermo Fischer Scientific) according to the manufacturer's protocols.

For knockdown experiments, RNA polymerase II–mediated RNAi expression vector plasmids were constructed using the BLOCK-iT Pol II miR RNAi Expression Vector kit (Thermo Fisher Scientific) according to the manufacturer's protocols. Target sequences were designed using software from the manufacturer's website (http://rnaidesigner.ThermoFisherScientific.com/rnaiexpress/rnaidesign.jsp). The following sequences were inserted: 5′-TGCTG*ACAGTAAGGCTGCCGGTG*GTTTTGGCCACTGAC TGACCACCGGCACTTACTGTAAT-3′ (KIF1Bα-miRNA) and 5′-TGC

Xu et al.
The KIF1Bβ kinesin transports IGF1R down the axon

Journal of Cell Biology
https://doi.org/10.1083/jcb.201801085

3491

TGTATAGATGAAGACGTAAGGGCGTTTTGGCCACTGACTGACGC
CCTTACCTTCATCTATA-3′ (KIF1Bβ-miRNA), in which the under-
lined nucleotides indicate the antisense target sequences. The
TurboRFP cDNA (Evrogen) was inserted before the 5′ miR-flank-
ing region as a marker of transfection. The specific knockdown
capacities were verified using IB. The target and TurboRFP cod-
ing sequences were subcloned into the *pCAGEN* vector (a kind
gift from Y. Gotoh, The University of Tokyo, Tokyo, Japan) for in
vitro electroporation.

Antibodies

The following antibodies were purchased from commer-
cial sources: anti-IGF1Rα mouse monoclonal antibody (RRID:
AB_10650003; sc-271606; Santa Cruz Biotechnology) diluted
1:500 for IB or 1:100 for immunofluorescence (IF); anti-IGF1Rβ
rabbit polyclonal antibody (RRID: AB_2122378; 3027; Cell Sig-
naling Technology) diluted 1:1,000 for IB; an anti–β-tubulin
III mouse monoclonal antibody (RRID: AB_532291; T5076; Sig-
ma-Aldrich) diluted 1:10,000 for IB or 1:500 for IF; anti–α-tubu-
lin mouse monoclonal antibody DM1A (RRID: AB_477593; T9026;
Sigma-Aldrich) diluted 1:1,000 for IB; anti-GFP rabbit polyclonal
antibody (RRID: AB_221569; A11122; Thermo Fisher Scientific)
diluted 1:1,000 for IB or 2 µg/ml for IP; anti-DENN/MADD rab-
bit monoclonal antibody (RRID: AB_2650580; ab134117; Abcam)
diluted 1:1,000 for IB or 1:100 for IF; antisynaptophysin mouse
monoclonal antibody (RRID: AB_94947; MAB368; EMD Milli-
pore) diluted 1:500 for IB; anti–DDDDK-tag mouse monoclonal
antibody (RRID: AB_11123930; M185-3L; MBL) diluted 1:1,000 for
IB; anti-Akt rabbit polyclonal antibody (RRID: AB_329827; 9272;
Cell Signaling Technology) diluted 1:1,000 for IF; anti–phos-
pho-Akt (Thr308; D25E6) rabbit monoclonal antibody (RRID:
AB_2629447; 13038; Cell Signaling Technology) diluted 1:500
for IF; anti-pERK (RRID: AB_331646; 9101; Cell Signaling Tech-
nology) diluted 1:500 for IF; anti–β-actin (RRID: AB_476744; Sig-
ma-Aldrich) diluted 1:10,000 for IB; normal rabbit IgG (catalog
55944; lot 07285; MP Cappel); Alexa fluor–labeled IgGs (Thermo
Fisher Scientific) diluted 1:200–500 for IF; and HRP-labeled IgGs
(GE Healthcare) diluted 1:1,000–3,000 for IB.

An anti-KIF1Bβ rabbit polyclonal antibody has previously
been described (RRID: AB_2571746; Zhao et al., 2001) and was
diluted 1:500 for IB. An anti-KIF1Bα rabbit polyclonal antibody
was raised against the synthetic peptide NQQPPPQLRWRSNSL
NNGQPKTTRC (1,037–1,061 aa; RRID:AB_2732865) and was di-
luted 1:500 for IB.

Histology

Mouse brain histology was performed as previously described
(Zhao et al., 2001). Briefly, the brains of mouse embryos at 18.5
dpc were fixed with FEA (5% neutral buffered formalin, 5% glacial
acetic acid, and 90% of 80% ethanol [vol/vol]) for 3 d. This pro-
cess was followed by dehydration with ethanol, clearance with
xylene, embedding in Paraplast (Sigma-Aldrich), and sectioning
with a Microm HM 355 microtome (speed = 15 mm/s, CONT V
= 15, thickness = 7–10 µm, temperature = 42°C, and water flow
= ~4). The sections were deparaffinized by xylene, rehydrated,
and then stained using Mayer's hematoxylin for 10 min to dis-
cern the nuclei. The sections were washed with deionized water,

stained with 0.3% eosin solution (water-soluble eosin) for 5 min,
dehydrated, processed with xylene, and mounted. The sections
were observed using a DM3000 upright microscope equipped
with 1.6×/0.05 and 10×/0.30 HCX Plan S-Apochromat objectives
(Leica Microsystems). Leica Application Suite (version 3.4.1) soft-
ware was used for imaging.

Primary culture of neurons

Hippocampal neurons were collected, dissociated, and cultured
as previously described (Niwa et al., 2008). Briefly, the hippo-
campi were dissected from the brains of 16.5–17.5 dpc mouse
embryos, digested with 0.25% trypsin for 15 min at 37°C, and
plated in a 35-mm dish with a round hole (D11130H; Matsunami),
LabTek chambered coverglass (Thermo Fisher Scientific), and a
combined device of cover glass (633153; Carolina) and microflu-
idic chambers (Xona Microfluidics; described below in detail),
which were precoated with polyethylenimine (Sigma-Aldrich)
and poly-L-lysine (Sigma-Aldrich). The neurons were cultured
in MEM (Gibco) containing 33.3 mM glucose, 1 mM sodium py-
ruvate, 2 mM GlutaMAX-I supplement (Thermo Fisher Scien-
tific), and 10% horse serum (Thermo Fisher Scientific) for 3–4 h
in a humid atmosphere with 5% CO_2 at 37°C. The medium was
changed to a medium with the same ingredients but with B27
supplement (Thermo Fisher Scientific) instead of horse serum.
To measure neuronal outgrowth with surface IF microscopy,
neurons were plated at $8.6 × 10^4$ cells/cm^2 and assayed at DIV2–3
to circumvent apoptosis (Niwa et al., 2008). To measure IGF-I
signaling, neurons were plated at $2.6–4.3 × 10^4$ cells/cm^2 and as-
sayed at DIV4. Mouse cortical neuron culture was performed as
previously described (Ichinose et al., 2015).

Microfluidic chamber culture

Microfluidic chamber culture was performed basically as previ-
ously described (Zhou et al., 2012). The coverslips (24 × 50 mm;
thickness 0.13–0.17 mm; 633153; Carolina) were washed by son-
ication for 30 min, rinsed with 70% ethanol and double-distilled
water (three times), and dried in a 50°C oven overnight. The
samples were further coated with poly-L-lysine overnight, which
was followed by a double-distilled water wash for 1 h three times,
and the samples were finally dried for ~15 min. During wash-
ing, the microfluidic chambers were sterilized with 70% ethanol
and dried for >1 h. Then, the dried cover glasses and microfluidic
chambers were combined and preincubated with MEM contain-
ing 33.3 mM glucose, 1 mM sodium pyruvate, 2 mM GlutaMAX-I
supplement, and 10% horse serum. Dissociated hippocampal
neurons were added to the left main channels of the chamber
as drops of 10 µl for two to three times at a concentration of ~6
$× 10^4$ cells/ml. The medium was changed to one containing B27
supplement 30 min after the cells were loaded. The medium was
then changed every 2 d.

Plasmid transfection

The dissociated cultured hippocampal neurons were trans-
fected using an improved calcium phosphate protocol at DIV1–6
(Jiang and Chen, 2006) or electroporation before plating using
a Neon transfection system (Thermo Fisher Scientific) with the
indicated constructs following to the manufacturer's protocol.

Briefly, 1 µg DNA was mixed with $4–8 \times 10^4$ neurons in 10 µl buffer and inserted in a 10 µl Neon Tip. Then, the electroporation was performed with the following conditions: pulse voltage = 1,400 V, pulse width = 20 ms, and pulse number = 1.

Yeast two-hybrid assays
Yeast two-hybrid assays were performed using the MatchMaker version 3 kit (Takara Bio Inc.) as previously described (Zhou et al., 2009). Five fragments of mouse *Kif1bβ* cDNA corresponding with aa 764–1,603, 885–1,410, 1,101–1,603, 1,411–1,603, 885–1,100, and 1,655–1,754 or mouse *Kif1a* 836–1,346-aa cDNA were ligated to the bait vector *pGBKT7* (Takara Bio Inc.). The ICD of mouse *Igf1r* (961–1,373 aa) was ligated with the prey vector *pGADT7* (Takara Bio Inc.). Yeast cells were cotransformed with each pair of bait and prey vectors, and the interaction between the fragments was assessed using α-galactosidase staining (Takara Bio Inc.) according to the Yeast Protocol Handbook (Takara Bio Inc.).

Vesicle IP and flotation assays
Vesicle IP and flotation assays were performed as previously described (Zhao et al., 2001; Tanaka et al., 2016). WT and *Kif-1bβ*[GFP/GFP] adult mouse brains were homogenized with ~5 ml Hepes-sucrose buffer (10 mM Hepes, pH 7.4, 320 mM sucrose, 5 mM $MgSO_4$, 1 mM EGTA, and protease inhibitors [cOmplete mini EDTA-free inhibitor; Roche]) and cleared by centrifugation twice at 1,000 *g* for 10 min at 4°C. For IP, the supernatant (S1) was mixed with 50 µl magnetic beads (µMACS Protein A; 130-042-601; Miltenyi Biotec) and 2 µg anti-GFP antibody for 2 h at 4°C. The beads were washed, eluted, and sampled for IB. For the flotation assay, the supernatant was diluted in 60% Nycodenz at a volume ratio of 1:5 and subjected to step-gradient ultracentrifugation with Nycodenz (0, 10, 20, 30, 40, 50, and 60%; Progen Biotechnik) in OptiSeal tubes (11.2 ml; 362181; Beckman Coulter) using an Optima XL-100K Ultracentrifuge with an NVT 65 rotor (Beckman Coulter) at 65,000 rpm for 2.5 h at 4°C with both acceleration and deceleration in the slowest mode of 9. The effluent fractions were collected by piercing the bottom of the tube with a 22G needle (NN-2238R; Terumo) and placing in 1.5-ml tubes at 500 µl/tube, and the fractions were subjected to IB.

Surface biotinylation
The cortical neurons of 17.5-dpc mouse brains were plated on 10-cm dishes at a density of 8.6×10^4 cells/cm² basically as previously described (Ichinose et al., 2015). The samples were subjected to a surface biotinylation assay at DIV7 as previously described (Tanaka et al., 2016) using the Pierce Cell Surface Protein Isolation kit (89881; Thermo Fisher Scientific) according to the manufacturer's protocols. The same amounts of protein in *Kif1b*^{+/+} and *Kif1b*^{−/−} lysates were subjected to the assay. The membrane fraction was loaded at the same ratio as the total protein fraction, which was normalized according to the β-actin level.

GST-pulldown assay
A GST-pulldown assay was performed basically as previously described (Zhao et al., 2001; Kanai et al., 2004). *Escherichia coli* strain BL21 was transformed with the respective GST-fused expression vectors and induced for protein expression with 0.5 mM IPTG at 16°C for 24 h when the OD_{600} reached 0.4–0.6. The bacteria were pelleted and subjected to a French Press after resuspension in buffer containing 50 mM Tris, pH 8.0, 0.5 M NaCl, 1% Triton X-100, and protease inhibitors (cOmplete mini EDTA-free inhibitor; Roche). The lysates were cleared by ultracentrifugation using an Optima XL-100K Ultracentrifuge with a 70Ti rotor (Beckman Coulter) at 50,000 rpm at 2°C for 0.5 h. The supernatant was divided into 1.5-ml tubes, snap frozen in liquid N_2, and then kept in a −80°C deep freezer for future use. Saturated amounts of lysates were loaded onto Glutathione Sepharose beads (17-0756-05; GE Healthcare), washed with WIBA (20 mM Tris, pH 8.5, 1 M NaCl, 1 mM Mg acetate, and 1% Triton X-100), and then washed with WIBB (20 mM Tris, pH 8.5, 1 mM Mg acetate, and 1% Triton X-100). Adult mouse brains were homogenized in buffer containing 20 mM Hepes, pH 7.4, 150 mM NaCl, 1% Triton X-100, 1 mM EGTA, and 1 mM Mg acetate. The S2 fraction was collected, precleared, and rotated with the beads at 4°C for 2 h. The beads were washed with homogenization buffer four times and subjected to IB analysis.

Pulldown of heterologously expressed KIF1Bβ885–1,410 by purified IGF1RβICD–3×FLAG
GST-tagged KIF1Bβ885–1,410 and GST alone were expressed in *E. coli* BL21 (DE3) and purified by affinity chromatography using Glutathione Sepharose 4B beads (GE Healthcare) followed by gel filtration through a Superdex 200 (GE Healthcare) size exclusion chromatography column. IGF1RβICD–3×FLAG was expressed in HEK 293 cells and extracted with lysis buffer (50 mM Tris, 150 mM NaCl, 0.1% Triton X-100, 0.05% CHAPS, and cOmplete, pH 8.0). An anti-FLAG M2 Affinity Gel (Merck) was incubated with the cell extracts for 1 h followed by three washes with the lysis buffer. Expression and purification of IGF1RβICD–3×FLAG was verified by IB. Purified GST or GST–KIF1Bβ885–1,410 was incubated with IGF1RβICD–3×FLAG-coated beads in TBS (50 mM Tris and 150 mM NaCl, pH 8.0) for 1 h. After washing the beads with the TBS three times, proteins were eluted with 200 µg/ml 3×FLAG peptide, subjected to 15% SDS-PAGE, and stained with Coomassie Brilliant Blue.

Human genome analyses
Two new independent pedigrees of CMT2A were diagnosed at the Neuromuscular Clinic of the Penn State Hershey Medical Center and Hamburg Center. Upon written informed consent and ethics committee approval at Pennsylvania State University and The University of Tokyo, the patient DNA samples were subjected to exome sequencing by Proprietary Next-Generation Sequencing technologies using the Illumina HiSeq 1500 platform. The Hereditary Neuropathy NextGen DNA Sequencing Panel included the following 33 genes (MIM numbers): *AARS* (601065), *ATL1* (606439), *DNM2* (602378), *DNMT1* (126375), *DYNC1H1* (600112), *EGR2* (129010), *FGD4* (611104), *GARS* (600287), *GDAP1* (606598), *GJB1* (304040), *GLA* (300644), *HSPB1* (602195), *HSPB8* (608014), *KIF1B* (605995), *LITAF* (603795), *LMNA* (150330), *LRSAM1* (610933), *MED25* (610197), *MFN2* (608507), *MPZ* (159440), *MTMR2* (603557), *NDRG1* (605262), *NEFL* (162280), *PMP22* (601097), *PRX* (605725), *RAB7A* (602298), *SBF2* (607697), *SCN9A* (603415), *SH3TC2* (608206), *SPT LC2* (605713), *TRPV4* (605427), *TTR* (176300), and *YARS* (603623).

Xu et al.
The KIF1Bβ kinesin transports IGF1R down the axon

Journal of Cell Biology 3493
https://doi.org/10.1083/jcb.201801085

IF microscopy

Immunocytochemistry was performed as previously described (Tanaka et al., 2016). Mouse hippocampal neurons at DIV2–4 were fixed in 4% PFA/PBS at 37°C for 10 min and directly blocked (for surface anti-IGF1Rα staining), or they were permeabilized first with 0.1% Triton X-100 or 1% saponin (for anti-IGF1Rα staining) in PBS, blocked using 1% normal goat serum/PBS, and incubated with primary antibodies overnight at 4°C in the blocking buffer (in the case of saponin, the detergent was added throughout the procedure). This was followed by PBS washes for 5 min each, thrice. They were then incubated with Alexa Fluor–labeled secondary antibodies (Thermo Fisher Scientific) diluted at 1:500 for 1 h at room temperature. They were washed three times with PBS for 5 min each and observed with confocal laser-scanning microscopy (LSM510, LSM5-Duo, LSM710, or LSM780 with Airyscan; ZEISS) equipped with the objectives (40×/1.4 Plan Apochromat oil immersion, 40×/1.3 Plan Apochromat oil immersion, 20×/0.8 Plan Apochromat, or 40×/1.2 C-Apochromat) or SR-SIM (model ELYRA S.1; ZEISS) equipped with an α Plan Apochromat objective (100×/1.46 oil immersion) at room temperature. The data acquisition was conducted by using Zen software (ZEISS). Fluorescent quantification was conducted using either ImageJ (National Institutes of Health) or MetaMorph (Molecular Devices) software.

Especially for pAkt IF staining, neurons were plated at a density of 4.3×10^4 cells/cm^2. At DIV3, they were starved for 2 h without serum or supplement and then stimulated by 5 nM IGF for 5 min. The cells were then immediately fixed in 4% PFA/PBS containing a phosphatase inhibitor cocktail (PhosSTOP; Roche) at 37°C for 10 min, stained after permeabilization using 0.1% Triton X-100 in PBS, and observed as described above.

For TUNEL staining, dissociated hippocampal neurons were fixed at DIV3 and subjected to TUNEL assays using the In Situ Cell Death Detection kit, Fluorescein (11684795910; Roche), following the manufacturer's protocols with counterstaining against βIII-tubulin.

For rescue experiments of membrane IGF1R staining, hippocampal neurons were plated at a density of 2.6×10^4 cells/cm^2 on 35-mm glass-bottom dishes (14-mm diameter hole; No.1S 0.16–0.19 mm; D11130H; Matsunami). The neurons were transfected with the respective rescue plasmids at DIV1 and fixed at DIV4 followed by anti-IGF1Rα immunostaining without permeabilization. The samples were imaged after postfixation.

Live imaging

The primary cultured hippocampal neurons of *Kif1bβ-EGFP*–knock-in mice were observed in the complete culture medium at room temperature on a ZEISS ELYRA.P1 total internal reflection fluorescence microscope with an α Plan Apochromat objective (100×/1.46 oil immersion). The SP-IGF1Rβ-RFP expression vector was cotransfected with the KIF1Bβ-EGFP expression vector into DIV6-dissociated cultured hippocampal neurons using the calcium phosphate method, and live imaging was similarly conducted at DIV7. The GFP and RFP signals were recorded in a humid 5% CO_2 atmosphere at 37°C on a spinning-disk confocal unit with an Andor iXon electron-multiplying charge-coupled device camera on an inverted ZEISS Axiophot microscope

equipped with 100×/1.46 Plan Apochromat oil immersion objective lens as previously described (Tanaka et al., 2016) or on an inverted ZEISS LSM780 confocal laser-scanning microscope with a Plan Apochromat oil-immersion objective (40×/1.3) sequentially with an exposure time of 500 ms. The data were collected with the Andor iQ2 or ZEISS Zen software and aligned with the ImageJ and MetaMorph software. Because of the time delay in sequential recording, RFP images of the comigration vesicles were continuously followed by the GFP images.

Superresolution microscopy

For organelle colocalization assay in Fig. 5, the immunostained samples were subjected to a SR-SIM (ELYRA PS.1) equipped with an oil-immersed α Plan Apochromat lens (100×/1.46) using Zen software and analyzed using ImageJ and MetaMorph software.

Statistics

Statistical analysis was performed in Prism 6 (GraphPad Software), Excel (Microsoft), and R software. Statistical tests, number of samples, and experiments are indicated in the figure legends. No statistical method was used to predetermine the sample size. For *t* tests, the normal distribution was not assumed according to Welch's method. Before the ANOVA tests, the normal distribution was tested using Kolmogorov–Smirnov test.

Online supplemental material

In Fig. S1, histological data and in vitro data are presented, suggesting that KIF1B deficiency or the KIF1Bβ Y1087C mutation impairs axon growth. In Fig. S2, the functional difference between KIF1Bβ and KIF1A, generation of *KIF1bβ$^{GFP/GFP}$* mice, and quantification of IGF1R transport on KIF1B deficiency are described. In Fig. S3, the effect of KIF1B deficiency on surface IGF1Rα levels is described. In Fig. S4, the effect of KIF1B deficiency or KIF1Bβ mutation on IGF-I–mediated ERK signaling is described. In Fig. S5, unchanged total Akt levels in RNAi experiments are shown. In Video 1, live imaging of a KIF1Bβ-EGFP–knock-in neuron is shown. In Video 2, comigration of KIF1Bβ and IGF1R is shown.

Acknowledgments

References

Baloh, R.H., R.E. Schmidt, A. Pestronk, and J. Milbrandt. 2007. Altered axonal mitochondrial transport in the pathogenesis of Charcot-Marie-Tooth disease from mitofusin 2 mutations. *J. Neurosci.* 27:422–430. https://doi.org/10.1523/JNEUROSCI.4798-06.2007

Baron-Van Evercooren, A., C. Olichon-Berthe, A. Kowalski, G. Visciano, and E. Van Obberghen. 1991. Expression of IGF-I and insulin receptor genes in the rat central nervous system: a developmental, regional, and cellular analysis. *J. Neurosci. Res.* 28:244–253. https://doi.org/10.1002/jnr.490280212

Beck, K.D., L. Powell-Braxton, H.R. Widmer, J. Valverde, and F. Hefti. 1995. *Igf1* gene disruption results in reduced brain size, CNS hypomyelination, and loss of hippocampal granule and striatal parvalbumin-containing neurons. *Neuron.* 14:717–730. https://doi.org/10.1016/0896-6273(95)90216-3

Bucci, C., O. Bakke, and C. Progida. 2012. Charcot-Marie-Tooth disease and intracellular traffic. *Prog. Neurobiol.* 99:191–225. https://doi.org/10.1016/j.pneurobio.2012.03.003

Busiguina, S., A.M. Fernandez, V. Barrios, R. Clark, D.L. Tolbert, J. Berciano, and I. Torres-Aleman. 2000. Neurodegeneration is associated to changes in serum insulin-like growth factors. *Neurobiol. Dis.* 7(6, 6 Pt B):657–665. https://doi.org/10.1006/nbdi.2000.0311

Camarero, G., C. Avendano, C. Fernandez-Moreno, A. Villar, J. Contreras, F. de Pablo, J.G. Pichel, and I. Varela-Nieto. 2001. Delayed inner ear maturation and neuronal loss in postnatal Igf-1-deficient mice. *J. Neurosci.* 21:7630–7641. https://doi.org/10.1523/JNEUROSCI.21-19-07630.2001

Castellano, E., and J. Downward. 2011. RAS interaction with PI3K: more than just another effector pathway. *Genes Cancer.* 2:261–274. https://doi.org/10.1177/1947601911408079

Castro, J., R.I. Garcia, S. Kwok, A. Banerjee, J. Petravicz, J. Woodson, N. Mellios, D. Tropea, and M. Sur. 2014. Functional recovery with recombinant human IGF1 treatment in a mouse model of Rett Syndrome. *Proc. Natl. Acad. Sci. USA.* 111:9941–9946. https://doi.org/10.1073/pnas.1311685111

Charalambous, D.C., E. Pasciuto, V. Mercaldo, P. Pilo Boyl, S. Munck, C. Bagni, and N. Santama. 2013. KIF1Bβ transports dendritically localized mRNPs in neurons and is recruited to synapses in an activity-dependent manner. *Cell. Mol. Life Sci.* 70:335–356. https://doi.org/10.1007/s00018-012-1108-0

Crowder, K.M., J.M. Gunther, T.A. Jones, B.D. Hale, H.Z. Zhang, M.R. Peterson, R.H. Scheller, C. Chavkin, and S.M. Bajjalieh. 1999. Abnormal neurotransmission in mice lacking synaptic vesicle protein 2A (SV2A). *Proc. Natl. Acad. Sci. USA.* 96:15268–15273. https://doi.org/10.1073/pnas.96.26.15268

Dentremont, K.D., P. Ye, A.J. D'Ercole, and J.R. O'Kusky. 1999. Increased insulin-like growth factor-I (IGF-I) expression during early postnatal development differentially increases neuron number and growth in medullary nuclei of the mouse. *Brain Res. Dev. Brain Res.* 114:135–141. https://doi.org/10.1016/S0165-3806(99)00024-3

Drew, A.P., D. Zhu, A. Kidambi, C. Ly, S. Tey, M.H. Brewer, A. Ahmad-Annuar, G.A. Nicholson, and M.L. Kennerson. 2015. Improved inherited peripheral neuropathy genetic diagnosis by whole-exome sequencing. *Mol. Genet. Genomic Med.* 3:143–154. https://doi.org/10.1002/mgg3.126

Dudek, H., S.R. Datta, T.F. Franke, M.J. Birnbaum, R. Yao, G.M. Cooper, R.A. Segal, D.R. Kaplan, and M.E. Greenberg. 1997. Regulation of neuronal survival by the serine-threonine protein kinase Akt. *Science.* 275:661–665. https://doi.org/10.1126/science.275.5300.661

Forcet, C., E. Stein, L. Pays, V. Corset, F. Llambi, M. Tessier-Lavigne, and P. Mehlen. 2002. Netrin-1-mediated axon outgrowth requires deleted in colorectal cancer-dependent MAPK activation. *Nature.* 417:443–447. https://doi.org/10.1038/nature748

Geppert, M., V.Y. Bolshakov, S.A. Siegelbaum, K. Takei, P. De Camilli, R.E. Hammer, and T.C. Südhof. 1994a. The role of Rab3A in neurotransmitter release. *Nature.* 369:493–497. https://doi.org/10.1038/369493a0

Geppert, M., Y. Goda, R.E. Hammer, C. Li, T.W. Rosahl, C.F. Stevens, and T.C. Südhof. 1994b. Synaptotagmin I: a major Ca^{2+} sensor for transmitter release at a central synapse. *Cell.* 79:717–727. https://doi.org/10.1016/0092-8674(94)90556-8

Gumy, L.F., G.S. Yeo, Y.C. Tung, K.H. Zivraj, D. Willis, G. Coppola, B.Y. Lam, J.L. Twiss, C.E. Holt, and J.W. Fawcett. 2011. Transcriptome analysis of embryonic and adult sensory axons reveals changes in mRNA repertoire localization. *RNA.* 17:85–98. https://doi.org/10.1261/rna.2386111

Hendricks, A.G., J.E. Lazarus, E. Perlson, M.K. Gardner, D.J. Odde, Y.E. Goldman, and E.L. Holzbaur. 2012. Dynein tethers and stabilizes dynamic microtubule plus ends. *Curr. Biol.* 22:632–637. https://doi.org/10.1016/j.cub.2012.02.023

Hirokawa, N., and Y. Tanaka. 2015. Kinesin superfamily proteins (KIFs): Various functions and their relevance for important phenomena in life and diseases. *Exp. Cell Res.* 334:16–25. https://doi.org/10.1016/j.yexcr.2015.02.016

Hirokawa, N., S. Niwa, and Y. Tanaka. 2010. Molecular motors in neurons: transport mechanisms and roles in brain function, development, and disease. *Neuron.* 68:610–638. https://doi.org/10.1016/j.neuron.2010.09.039

Ho, C.C., S.M. Tai, E.C. Lee, T.S. Mak, T.K. Liu, V.W. Tang, and W.T. Poon. 2017. Rapid Identification of Pathogenic Variants in Two Cases of Charcot-Marie-Tooth Disease by Gene-Panel Sequencing. *Int. J. Mol. Sci.* 18:770. https://doi.org/10.3390/ijms18040770

Hodge, R.D., A.J. D'Ercole, and J.R. O'Kusky. 2005. Increased expression of insulin-like growth factor-I (IGF-I) during embryonic development produces neocortical overgrowth with differentially greater effects on specific cytoarchitectonic areas and cortical layers. *Brain Res. Dev. Brain Res.* 154:227–237. https://doi.org/10.1016/j.devbrainres.2004.10.016

Huebner, E.A., and S.M. Strittmatter. 2009. Axon regeneration in the peripheral and central nervous systems. *Results Probl. Cell Differ.* 48:339–351.

Ichinose, S., T. Ogawa, and N. Hirokawa. 2015. Mechanism of Activity-Dependent Cargo Loading via the Phosphorylation of KIF3A by PKA and CaMKIIa. *Neuron.* 87:1022–1035. https://doi.org/10.1016/j.neuron.2015.08.008

Janz, R., Y. Goda, M. Geppert, M. Missler, and T.C. Südhof. 1999. SV2A and SV2B function as redundant Ca^{2+} regulators in neurotransmitter release. *Neuron.* 24:1003–1016. https://doi.org/10.1016/S0896-6273(00)81046-6

Jiang, M., and G. Chen. 2006. High Ca^{2+}-phosphate transfection efficiency in low-density neuronal cultures. *Nat. Protoc.* 1:695–700. https://doi.org/10.1038/nprot.2006.86

Jones, D.M., B.A. Tucker, M. Rahimtula, and K.M. Mearow. 2003. The synergistic effects of NGF and IGF-1 on neurite growth in adult sensory neurons: convergence on the PI 3-kinase signaling pathway. *J. Neurochem.* 86:1116–1128. https://doi.org/10.1046/j.1471-4159.2003.01925.x

Kanai, Y., N. Dohmae, and N. Hirokawa. 2004. Kinesin transports RNA: isolation and characterization of an RNA-transporting granule. *Neuron.* 43:513–525. https://doi.org/10.1016/j.neuron.2004.07.022

Kijima, K., C. Numakura, H. Izumino, K. Umetsu, A. Nezu, T. Shiiki, M. Ogawa, Y. Ishizaki, T. Kitamura, Y. Shozawa, and K. Hayasaka. 2005. Mitochondrial GTPase mitofusin 2 mutation in Charcot-Marie-Tooth neuropathy type 2A. *Hum. Genet.* 116:23–27. https://doi.org/10.1007/s00439-004-1199-2

Kuemmerle, J.F., and K.S. Murthy. 2001. Coupling of the insulin-like growth factor-I receptor tyrosine kinase to G$_{i2}$ in human intestinal smooth muscle: G$_{βγ}$-dependent mitogen-activated protein kinase activation and growth. *J. Biol. Chem.* 276:7187–7194. https://doi.org/10.1074/jbc.M011145200

Kuemmerle, J.F., and K.S. Murthy. 2001. Coupling of the insulin-like growth factor-I receptor tyrosine kinase to G$_i$2 in human intestinal smooth muscle: G$_{βγ}$-dependent mitogen-activated protein kinase activation and growth. *J. Biol. Chem.* 276:7187–7194. https://doi.org/10.1074/jbc.M011145200

Laurino, L., X.X. Wang, B.A. de la Houssaye, L. Sosa, S. Dupraz, A. Cáceres, K.H. Pfenninger, and S. Quiroga. 2005. PI3K activation by IGF-1 is essential for the regulation of membrane expansion at the nerve growth cone. *J. Cell Sci.* 118:3653–3662. https://doi.org/10.1242/jcs.02490

Lawson, V.H., B.V. Graham, and K.M. Flanigan. 2005. Clinical and electrophysiologic features of CMT2A with mutations in the mitofusin 2 gene. *Neurology.* 65:197–204. https://doi.org/10.1212/01.wnl.0000168898.76071.70

Liu, J.P., J. Baker, A.S. Perkins, E.J. Robertson, and A. Efstratiadis. 1993. Mice carrying null mutations of the genes encoding insulin-like growth factor I (Igf-1) and type 1 IGF receptor (Igf1r). *Cell.* 75:59–72.

Liu, W., P. Ye, J.R. O'Kusky, and A.J. D'Ercole. 2009. Type 1 insulin-like growth factor receptor signaling is essential for the development of the hippocampal formation and dentate gyrus. *J. Neurosci. Res.* 87:2821–2832. https://doi.org/10.1002/jnr.22129

Lu, X., F. Kambe, X. Cao, M. Yamauchi, and H. Seo. 2008. Insulin-like growth factor-I activation of Akt survival cascade in neuronal cells requires the presence of its cognate receptor in caveolae. *Exp. Cell Res.* 314:342–351. https://doi.org/10.1016/j.yexcr.2007.10.013

Luigetti, M., G.M. Fabrizi, G. Bisogni, A. Romano, F. Taioli, M. Ferrarini, D. Bernardo, P.M. Rossini, and M. Sabatelli. 2016. Charcot-Marie-Tooth type 2 and distal hereditary motor neuropathy: Clinical, neurophysiological and genetic findings from a single-centre experience. *Clin. Neurol. Neurosurg.* 144:67–71. https://doi.org/10.1016/j.clineuro.2016.03.007

Lyons, D.A., S.G. Naylor, A. Scholze, and W.S. Talbot. 2009. Kif1b is essential for mRNA localization in oligodendrocytes and development of myelinated axons. *Nat. Genet.* 41:854–858. https://doi.org/10.1038/ng.376

Massagué, J., and M.P. Czech. 1982. The subunit structures of two distinct receptors for insulin-like growth factors I and II and their relationship to the insulin receptor. *J. Biol. Chem.* 257:5038–5045.

McMahon, H.T., V.Y. Bolshakov, R. Janz, R.E. Hammer, S.A. Siegelbaum, and T.C. Südhof. 1996. Synaptophysin, a major synaptic vesicle protein, is not essential for neurotransmitter release. *Proc. Natl. Acad. Sci. USA.* 93:4760–4764. https://doi.org/10.1073/pnas.93.10.4760

Mishina, M., and K. Sakimura. 2007. Conditional gene targeting on the pure C57BL/6 genetic background. *Neurosci. Res.* 58:105–112. https://doi.org/10.1016/j.neures.2007.01.004

Nakafuku, M., T. Satoh, and Y. Kaziro. 1992. Differentiation factors, including nerve growth factor, fibroblast growth factor, and interleukin-6, induce an accumulation of an active Ras.GTP complex in rat pheochromocytoma PC12 cells. *J. Biol. Chem.* 267:19448–19454.

Niwa, S., Y. Tanaka, and N. Hirokawa. 2008. KIF1Bbeta- and KIF1A-mediated axonal transport of presynaptic regulator Rab3 occurs in a GTP-dependent manner through DENN/MADD. *Nat. Cell Biol.* 10:1269–1279. https://doi.org/10.1038/ncb1785

O'Kusky, J., and P. Ye. 2012. Neurodevelopmental effects of insulin-like growth factor signaling. *Front. Neuroendocrinol.* 33:230–251. https://doi.org/10.1016/j.yfrne.2012.06.002

O'Kusky, J.R., P. Ye, and A.J. D'Ercole. 2000. Insulin-like growth factor-I promotes neurogenesis and synaptogenesis in the hippocampal dentate gyrus during postnatal development. *J. Neurosci.* 20:8435–8442. https://doi.org/10.1523/JNEUROSCI.20-22-08435.2000

Özdinler, P.H., and J.D. Macklis. 2006. IGF-I specifically enhances axon outgrowth of corticospinal motor neurons. *Nat. Neurosci.* 9:1371–1381. https://doi.org/10.1038/nn1789

Raivich, G., and M. Makwana. 2007. The making of successful axonal regeneration: genes, molecules and signal transduction pathways. *Brain Res. Brain Res. Rev.* 53:287–311. https://doi.org/10.1016/j.brainresrev.2006.09.005

Recio-Pinto, E., M.M. Rechler, and D.N. Ishii. 1986. Effects of insulin, insulin-like growth factor-II, and nerve growth factor on neurite formation and survival in cultured sympathetic and sensory neurons. *J. Neurosci.* 6:1211–1219. https://doi.org/10.1523/JNEUROSCI.06-05-01211.1986

Saporta, A.S., S.L. Sottile, L.J. Miller, S.M. Feely, C.E. Siskind, and M.E. Shy. 2011. Charcot-Marie-Tooth disease subtypes and genetic testing strategies. *Ann. Neurol.* 69:22–33. https://doi.org/10.1002/ana.22166

Scolnick, J.A., K. Cui, C.D. Duggan, S. Xuan, X.B. Yuan, A. Efstratiadis, and J. Ngai. 2008. Role of IGF signaling in olfactory sensory map formation and axon guidance. *Neuron.* 57:847–857. https://doi.org/10.1016/j.neuron.2008.01.027

Skre, H. 1974. Genetic and clinical aspects of Charcot-Marie-Tooth's disease. *Clin. Genet.* 6:98–118. https://doi.org/10.1111/j.1399-0004.1974.tb00638.x

Sosa, L., S. Dupraz, L. Laurino, F. Bollati, M. Bisbal, A. Cáceres, K.H. Pfenninger, and S. Quiroga. 2006. IGF-1 receptor is essential for the establishment of hippocampal neuronal polarity. *Nat. Neurosci.* 9:993–995. https://doi.org/10.1038/nn1742

Sullivan, K.A., B. Kim, and E.L. Feldman. 2008. Insulin-like growth factors in the peripheral nervous system. *Endocrinology.* 149:5963–5971. https://doi.org/10.1210/en.2008-1020

Takemura, R., T. Nakata, Y. Okada, H. Yamazaki, Z. Zhang, and N. Hirokawa. 1996. mRNA expression of KIF1A, KIF1B, KIF2, KIF3A, KIF3B, KIF4, KIF5, and cytoplasmic dynein during axonal regeneration. *J. Neurosci.* 16:31–35. https://doi.org/10.1523/JNEUROSCI.16-01-00031.1996

Tanaka, Y., S. Niwa, M. Dong, A. Farkhondeh, L. Wang, R. Zhou, and N. Hirokawa. 2016. The Molecular Motor KIF1A Transports the TrkA Neurotrophin Receptor and Is Essential for Sensory Neuron Survival and Function. *Neuron.* 90:1215–1229. https://doi.org/10.1016/j.neuron.2016.05.002

Ueno, H., X. Huang, Y. Tanaka, and N. Hirokawa. 2011. KIF16B/Rab14 molecular motor complex is critical for early embryonic development by transporting FGF receptor. *Dev. Cell.* 20:60–71. https://doi.org/10.1016/j.devcel.2010.11.008

Ververis, J.J., L. Ku, and P. Delafontaine. 1993. Regulation of insulin-like growth factor I receptors on vascular smooth muscle cells by growth factors and phorbol esters. *Circ. Res.* 72:1285–1292. https://doi.org/10.1161/01.RES.72.6.1285

Wu, Z., A. Ghosh-Roy, M.F. Yanik, J.Z. Zhang, Y. Jin, and A.D. Chisholm. 2007. Caenorhabditis elegans neuronal regeneration is influenced by life stage, ephrin signaling, and synaptic branching. *Proc. Natl. Acad. Sci. USA.* 104:15132–15137. https://doi.org/10.1073/pnas.0707001104

Zhao, C., J. Takita, Y. Tanaka, M. Setou, T. Nakagawa, S. Takeda, H.W. Yang, S. Terada, T. Nakata, Y. Takei, et al. 2001. Charcot-Marie-Tooth disease type 2A caused by mutation in a microtubule motor KIF1Bbeta. *Cell.* 105:587–597. https://doi.org/10.1016/S0092-8674(01)00363-4

Zhou, B., Q. Cai, Y. Xie, and Z.H. Sheng. 2012. Snapin recruits dynein to BDNF-TrkB signaling endosomes for retrograde axonal transport and is essential for dendrite growth of cortical neurons. *Cell Reports.* 2:42–51. https://doi.org/10.1016/j.celrep.2012.06.010

Zhou, R., S. Niwa, N. Homma, Y. Takei, and N. Hirokawa. 2009. KIF26A is an unconventional kinesin and regulates GDNF-Ret signaling in enteric neuronal development. *Cell.* 139:802–813. https://doi.org/10.1016/j.cell.2009.10.023

Züchner, S., I.V. Mersiyanova, M. Muglia, N. Bissar-Tadmouri, J. Rochelle, E.L. Dadali, M. Zappia, E. Nelis, A. Patitucci, J. Senderek, et al. 2004. Mutations in the mitochondrial GTPase mitofusin 2 cause Charcot-Marie-Tooth neuropathy type 2A. *Nat. Genet.* 36:449–451. https://doi.org/10.1038/ng1341